MULLARD LIMITED
Mullard House
Torrington Place
London, W.C.1

CONTENTS

Introduction and References 198

Magnadur Permanent Magnets in small D.C. Motors with Three-pole Armatures 199-211

Design of small D.C. Motors embodying Magnadur Permanent Magnets 212-223

Flux Values in D.C. Motors embodying Magnadur Permanent Magnets 224-228

VOL. 8 No. 77 SEPTEMBER 1965

Mullard Technical Communications

VOLUME 8 NUMBER 77

September 1965

Mullard Technical Communications

VOLUME 8 NUMBER 77 September 1965

Contents

Introduction and References 198

Magnadur Permanent Magnets in small D.C. Motors with Three-pole Armatures *J. Koch, H. Wullkopf* 199

Design of small D.C. Motors embodying Magnadur Permanent Magnets *M. F. Reynst* 212

Flux Values in D.C. Motors embodying Magnadur Permanent Magnets *H. Wullkopf* 224

Mullard Technical Communications contains information on the performance or application of Mullard products such as electronic valves and tubes, semiconductor devices, and electrical and magnetic components. It is issued free-of-charge to equipment designers, research organisations, reference libraries, and educational establishments. Bona fide applications to be added to the circulation list should be made under an official letter head to Central Technical Services. Overseas enquiries should be addressed to the local Mullard agent, or to Mullard Overseas Ltd. at Mullard House.

Abstracts, or references to an article, should mention both the source, *Mullard Technical Communications*, and the authors. Requests for republication or translation should be made to the Editor in writing.

The issue of the information contained in this publication does not imply any authority or licence for the utilisation of any patented feature.

'Mullard' is the trade mark of Mullard Limited and is registered in most of the principal countries of the world.

Editor: F. A. Sowan

Assistant Editors: R. Barrie E. G. Evans F. Mills

Published by

Central Technical Services
Mullard Limited, Mullard House, Torrington Place, London, W.C.1
LANgham 6633

© Mullard Limited, 1965

Made and Printed in England by
WIGHTMAN AND COMPANY LIMITED, 1/3 BRIXTON ROAD, LONDON, S.W.9

INTRODUCTION

This issue comprises three articles on the design of small d.c. motors in which the field excitation is provided by permanent magnets – specifically, by magnets made from the ceramic material Magnadur.

The first article is a detailed analysis of the problem of 'pole sensitivity' in motors employing three-pole armatures, and it discusses the relative merits of different methods of magnetising the magnet system. The second is concerned with the practical design of small d.c. motors, and offers a design procedure that has certain advantages over conventional procedures. The third gives details of a method of calculating the magnetic flux passing through the armature, thus enabling the designer to determine the performance required from the magnet system.

These articles appeared originally, in German, in Valvo Berichte Vol. 10, No. 4, October 1964. The units that were employed by the authors have been retained. It should be noted that:

$$1 \text{ gauss} = 10^{-8} \text{ Vs/cm}^2$$

and that the unit of torque, the pond . centimetre (abbreviated pcm), is defined by

$$1 \text{ pond} \simeq 9{\cdot}807 \, \frac{\text{m . g}}{\text{s}^2},$$

the average acceleration due to gravity being approximately 9·807 m/s^2. (See also Kaye and Laby, 12th ed., page 9).

Reference is made to the performances obtainable with various grades of Magnadur. Magnets made from Magnadur grades 1, 2, or 3 are commercially available. Grades 2 (improved version) and 3 (improved version) are experimental variants of grades 2 and 3 respectively. The designations 2 (improved version) and 3 (improved version) have been adopted solely for the purposes of this publication; and they should not be regarded as present or future commercial type-numbers.

REFERENCES

1. Sequenz, H. 'Sonderbauarten von Kleinstmotoren'. **Elektrotechnik und Maschinenbau,** Vol. 62, July 1944, pp. 317 to 333.
2. Binder, U. 'Kleinste Elektromotoren'. **VDI Zeitschrift** (Verein Deutscher Ingenieure, Dusseldorf), Vol. 99, March 1957, pp. 383 to 388.
3. Fahlenbrach, H., and Sommerkorn, G. "Dauermagnete in Kleinmotoren'. **Elektrotechnische Zeitschrift A,** Vol. 75, May 1954, pp. 299 to 303.
4. Mohr, A. W. 'Bemessung von Dauermagneten für kleinste Gleichstrommotoren'. **Elektrotechnische Zeitschrift A,** Vol. 82, July 1961, pp. 481 to 485.
5. Brinkmann, K. 'Drehzal und maximaler Wirkungsgrad bei Gleichstrom-Kleinstmotoren'. **Elektrotechnische Zeitschrift A,** Vol. 83, Sep. 1962, pp. 665 to 668.
6. Janssen, H. J. "Gesichtspunkte für die Lärmbekämpfung bei Geräten mit Elektrokleinstmotoren'. **Elektrotechnik,** Vol. 32, 1962, pp. 482 to 484.
7. Wullkopf, H. 'Magnetische Synchronkupplungen aus Ferroxdure 100'. **Valvo-Berichte,** Vol. 8, No. 4, Nov. 1962, pp. 101 to 109.
8. Koch, J. 'Berechnung von Dauermagneten unter besonderer Berücksichtigung des Streufaktors'. **Valvo-Berichte,** Vol. 7, No. 5, Dec. 1961, pp. 131 to 158.
9. Wullkopf, H. See pages 224 to 228 of the present publication.
10. Spreadbury, F. G. 'Fractional h.p. Electric Motors'. Pitman, 1951.
11. Liwschitz-Garik, M., and Whipple, C. C. 'Direct-Current Machines'. Van Nostrand, 1956.
12. Metzler, K. 'Der Entwurf kleiner zweipoliger Gleichstrommotoren'. **Elektrotechnik,** Vol. 4, 1950, pp. 278 to 283.
13. Bolz, G. 'Drehschub und Hauptabmessungen der Gleichstromkleinstmaschinen'. **Elektrotechnische Zeitschrift,** Vol. 65, Sep. 1944, pp. 297 to 299.
14. Puchstein, A. F. 'Design of Small d.c. Motors: calculation, output, performance'. Wiley, 1961.
15. Koch, J., and Wullkopf, H. See pages 199 to 211 of the present publication.
16. Reynst, M. F. See pages 212 to 223 of the present publication.

Magnadur Permanent Magnets in small D.C. Motors with Three-pole Armatures

J. Koch and H. Wullkopf
Valvo GmbH, Hamburg

More and more small d.c. motors are being equipped with permanent magnets providing the field excitation. In motors of this kind having an armature of the three-pole type (usual for ratings up to 3W, and at the most 10W), what is known as 'pole sensitivity' becomes troublesome in many applications, signifying a dependence of torque on armature angle, which makes a higher starting voltage necessary.

In the present article, the torque delivered by a three-pole motor with permanent-magnet field excitation is calculated by a procedure that clearly explains pole sensitivity and its dependence on the magnetisation process. A method is presented whereby pole sensitivity can be minimised without appreciably reducing the delivered torque.

INTRODUCTION

Direct-current motors have been manufactured now for more than a century (Ref. 1). Permanent-magnet field excitation has mainly been employed in small motors. The overall size of such motors is less than that of motors embodying electromagnets (Ref. 2); the chief consideration being, that these very small designs are easier and cheaper to manufacture (Refs. 3, 4). Moreover, many d.c. motors of modern design, with permanent-magnet field excitation, have a higher efficiency than electromagnetically-excited types of the same size (Refs. 4, 5).

Of the many types of electric motor available, those embodying a ring magnet or segments made of Magnadur (Fig. 1) are of special interest, because they can be produced at a very reasonable price, particularly when miniaturised. It is also possible to design motors of this kind which, despite their high efficiency and torque, are comparatively free of pole sensitivity. This latter term will be used here in the sense of a periodic fluctuation in the total torque acting on the armature. The torque developed is, in fact, dependent on the position of the armature. It is further necessary to distinguish between 'electromagnetic pole sensitivity' and 'permanent-magnetic pole sensitivity': the first signifies a fluctuation in the torque as created by flux linkage between the main field and that of the current through the armature coils; the second effect, generally superimposed upon the first, is the tendency for the armature, when not energised, to remain in certain preferential positions determined by the main field.

It is, above all, in the motors of battery-operated record-players that pole sensitivity is troublesome (Ref. 6), since it is desirable that the turning moment should be as independent as possible of the turntable position. Pole sensitivity is also undesirable in battery-operated clocks, since these must be capable of starting at very small voltages; for example, when the battery is almost exhausted. However, a decrease in pole sensitivity, achieved by choosing a suitable magnetisation process, must not entail any appreciable fall-off in the torque delivered. In the somewhat larger motors used in motor vehicles for powering fans and windscreen-wipers, pole sensitivity plays only a minor part; by suitable magnetisation of the ring magnets, motors of this kind can be built to deliver torques that are quite large in relation to their size, and here a certain degree of pole sensitivity is of little account. A favourable factor in such designs is that the permanent magnets do not require an energising current that would otherwise contribute to temperature rise. These larger types of motor are also cheap to make, and they usually have high efficiency.

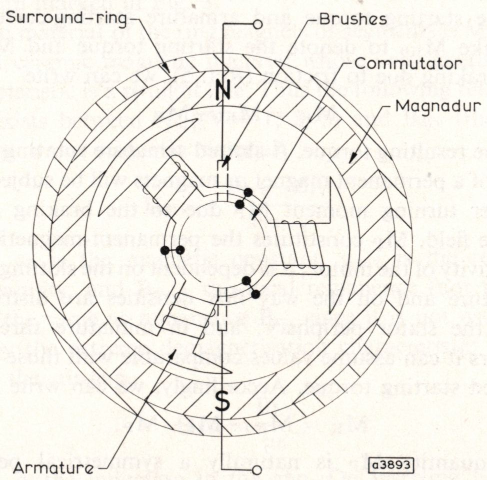

Fig. 1—Small d.c. motor with three-pole armature and Magnadur ring-magnet

In the following, a summary is given of the characteristics important in the design of miniature motors embodying ring segments. They are calculated as functions of geometrical dimensions and of the form of magnetisation of the rings or segments. Some of the results are compared with those obtained by measurement. Different fields of application call for different sets of requirements for electric motors, and these in their turn imply, generally speaking, two different forms of magnetisation, which will be examined in the present article. We shall only be concerned with miniature motors having armatures of the three-pole type. This type of armature, having only three slots, is particularly liable to pole sensitivity, an effect that is scarcely apparent in armatures having more than ten slots.

In the design calculations of miniature three-pole motors it has been found necessary to adopt an approach somewhat different from that usual in electric motor design: determination of torque must take into account the shape of the armature. The calculations are much simpler in a case where the armature is more or less solid, with a large number of small slots; for all that is necessary here is to work on the total amount of magnetic flux passing through the armature.

There are also marked differences between the applications for which three-pole motors are suitable and those for larger motors having multi-slot armatures. Almost all motors rated to deliver up to about 3W and not more than 10W mechanical power are equipped with three-pole armatures; the motors in question are generally battery-operated, and used for driving record-players, clocks, toys, etc. Somewhat larger machines with outputs ranging between 10W and 100W are equipped with multi-slot armatures (generally more than eight slots). These motors are powered from accumulators or higher-powered generators.

INFLUENCE OF FRICTION AND POLE SENSITIVITY ON THE DELIVERED TORQUE

In the small motors dealt with in this article the relation between torque and armature current cannot be one of straightforward proportion, because of the relative importance of brush and bearing friction. The same applies to the starting torque and armature starting-current. If we take M_{K0} to denote the starting torque and M_R for the braking due to friction (Ref. 5), we can write

$$M_K = M_{K0} - M_R$$

for the resulting torque. A slotted armature rotating in the field of a permanent magnet or magnets will be subject to a further turning moment M_P due to the braking action of the field. M_P constitutes the permanent-magnetic pole sensitivity of the motor; it is dependent on the slotting of the armature and on the way flux densities are distributed over the stator periphery; and in miniature three-pole motors it can assume values comparable with those of the desired starting torque. Accordingly, we can write

$$M_K = M_{K0} - M_R - M_P. \qquad \ldots(1)$$

The quantity M_P is naturally a symmetrical periodic function, similar to the couples occurring in magnetic synchronous clutches (Ref. 7). Averaged out over one revolution of the armature, the couple neither consumes nor creates energy, in which respect it contrasts with that due to friction, M_R. The implication is that permanent-magnetic pole sensitivity has no effect on the operation of the motor other than to set up this couple which is dependent on armature angle, and which may on occasion prove troublesome; but neither the efficiency nor the speed of the motor is affected. The existence of this couple serves to explain the big discrepancy found between the short-circuit torque as directly measured with the armature stalled, and the value obtained by extrapolation of the motor characteristic, a discrepancy that is particularly notable in small d.c. motors equipped with three-pole armatures.

Since pole sensitivity is a function of the form of magnetisation employed it is necessary to know how the magnetic flux is distributed along the periphery of the ring magnet. One way of carrying out the measurements is by sampling a set of points with a search coil and a ballistic galvanometer. The same sort of measurement can be carried out with a Hall probe, which is small in comparison with the object under investigation. Thus one can carry out direct measurements of the radial component of magnetic induction as a function-of-place. It is these radial-component values that are required in the design calculations. On page 208 the results of such measurements are compared with the calculated distribution of flux density.

CONSTRUCTION AND MODE OF FUNCTIONING OF A THREE-POLE MOTOR

The stator of the motor appearing in Fig. 1 consists of a Magnadur ring magnet and a soft-iron ring having a wall thickness sufficient to avoid saturation. The armature is of the three-pole type. The diagram shows how the coils are wound on the three pole-pieces and how they are connected up to the commutator. Current is supplied through two diametrically opposed brushes. It can further be inferred from the drawing that the end of one of the pole-pieces represents a north pole while the ends of the other two represent south poles, or vice versa. The windings on the two pole-pieces having the same polarity are connected up in series, and are parallel to that on the third pole-piece. If each pole-piece carries the same number of turns, it follows that the current through the windings on pole-pieces having the same polarity will always be half that flowing through the third winding. That is to say, if the total current through the armature is I, then I/3 will flow through the two series windings and 2I/3 through the shunt winding.

In a series of diagrams (a) (b) (c) (d) (e) (f), Fig. 2 shows schematically the changes of magnetic polarity during one revolution of the armature. In diagram (a) it is assumed that pole-piece 1 for the time being has south polarity and is accordingly attracted to the north pole of the field magnet; pole-piece 2, a north pole, is repelled by the same field-magnet pole. Pole-piece 3 is also a north pole and has a position a little in front of the central point of the field magnet south pole, and so undergoes a pull toward that point. Once pole-piece 3 has passed that point it becomes a south pole, diagram (b), in consequence of commutation, and is repelled by the south pole of the field magnet. At the same time, changes occur in the currents energising the other two windings. The winding on pole-piece 1 previously carried a current of 2I/3 and now carries one of I/3; with pole-piece 2 it is the other way about. Pole-piece 1, now in the vicinity of the central point of the field magnet north, becomes a north pole on passing that point (diagram c) and is accordingly repulsed. The changes just described affect one pole-piece after another as the armature passes through the three further positions represented in diagrams (d), (e), and (f). The essential point is, that it is always the pole-piece that is passing the centre of a field magnet pole that undergoes a reversal of polarity. The force acting on any one pole-piece irrespective of position, always has the same direction and always contributes to the total torque developed.

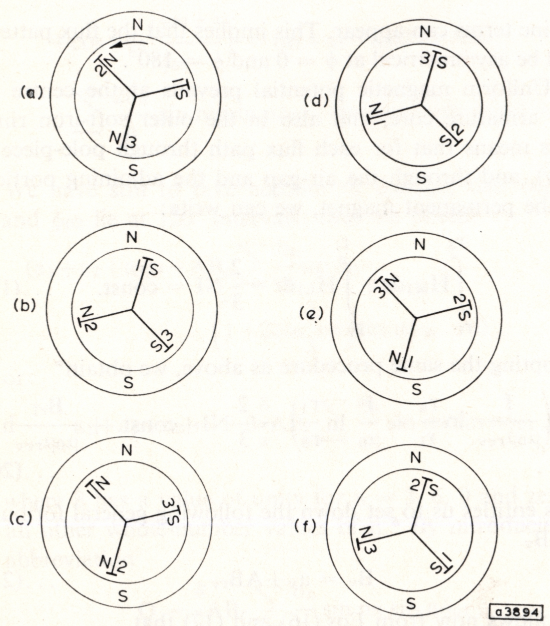

Fig. 2—Changes of polarity during one revolution of the motor shown in Fig. 1

RADIAL MAGNETISATION

Calculation of Torque

Now that the principle on which a three-pole motor functions has been explained we can proceed to calculate the torque it develops. In so doing we shall make use of Ampere's Law ($\oint H ds = NI$, where N is the number of turns) and the principle of the vanishing divergence of magnetic induction (div B = 0). Both in the iron of the armature core and in the soft-iron ring that encloses the ring magnet, permeabilities are very high and field strengths are therefore very low, so that we can consistently neglect the contribution to the ring integral for which the soft iron is responsible. We shall suppose the field strength and induction to have the direction indicated in Fig. 3, and take 2α to denote the angle subtended by the broad end of a pole-piece to the centre of the system.

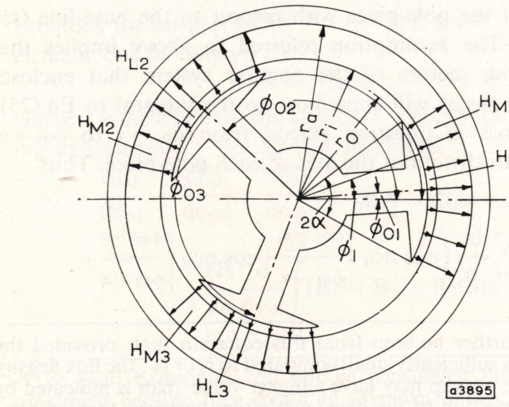

Fig. 3—Field pattern for radial magnetisation

Let us first consider the radial magnetisation. The result of the process should be that B and H, at every point of the magnet, possess only radial components (Fig. 3). We shall further assume that the same applies to field and induction values in the air-gap. There is in fact quite good justification for making this assumption where the air-gaps are narrow and the motor is equipped with an iron armature core, for the lines of magnetic force issue from the iron more or less perpendicularly, on account of its high permeability. Components of induction running tangentially to the surface would not, in any case, contribute to the forces acting on the armature.

Accordingly, for the ring integrals passing through pole-pieces 1 and 2 and through pole-pieces 1 and 3 we have

$$-\int_{r_i}^{r_a} H_{M1}dr - \int_{r_0}^{r_i} H_{L1}dr + \int_{r_i}^{r_a} H_{M2}dr + \int_{r_0}^{r_i} H_{L2}dr = \\ = -\frac{2}{3}NI - \frac{1}{3}NI, \qquad \ldots(2)$$

$$-\int_{r_i}^{r_a} H_{M1}dr - \int_{r_0}^{r_i} H_{L1}dr + \int_{r_i}^{r_a} H_{M3}dr + \int_{r_0}^{r_i} H_{L3}dr = \\ = -\frac{2}{3}NI - \frac{1}{3}NI. \qquad \ldots(3)$$

The symbols H_{M1}, H_{M2} and H_{M3} denote field strengths at any point in the magnet material facing pole-pieces 1, 2, and 3; namely, at any point lying within the subtended angle 2α, H_{L1}, H_{L2}, and H_{L3} are field-strengths at corresponding points in the air-gaps, and r_a, r_i and r_0 are the radii marked in Fig. 3.

The material of the ring magnets or segments is Magnadur, a ceramic magnetic material whose demagnetisation characteristic is a straight line. Thus the following relationship exists between H_{Mv}(V = 1, 2, 3) and B_{Mv} (the flux density in the magnetic material):

$$H_{Mv} = \frac{B_{Mv} - B_{rv}}{\mu_0 \mu_{rev}}, \qquad \ldots(4)$$

where μ_0 is the magnetic constant, μ_{rev} is the reverse permeability, and B_{rv}, the local remanence (not necessarily the same as remanence B_r, since it is not usual to employ the extreme demagnetisation characteristic here).

In the air-gap,

$$H_{Lv} = \frac{B_{Lv}}{\mu_0}, \qquad \ldots(5)$$

if B_{Lv} is the induction in the gap. On inserting Eqs.(4) and (5) into Eq.(2) and (3) we obtain

$$\int_{r_i}^{r_a} \frac{B_{M1} - B_{r1}}{\mu_0 \mu_{rev}} dr + \int_{r_0}^{r_i} \frac{B_{L1}}{\mu_0} dr - \int_{r_i}^{r_a} \frac{B_{M2} - B_{r2}}{\mu_0 \mu_{rev}} dr - \int_{r_0}^{r_i} \frac{B_{L2}}{\mu_0} dr = NI, \qquad \ldots(6)$$

$$\int_{r_i}^{r_a} \frac{B_{M1} - B_{r1}}{\mu_0 \mu_{rev}} dr + \int_{r_0}^{r_i} \frac{B_{L1}}{\mu_0} dr - \int_{r_i}^{r_a} \frac{B_{M3} - B_{r3}}{\mu_0 \mu_{rev}} dr - \int_{r_0}^{r_i} \frac{B_{L3}}{\mu_0} dr = NI. \qquad \ldots(7)$$

Over $\Delta\alpha$, a small section of the system made up of magnet material and air-gap, the flux is constant; moreover, the cross-sections through which the flux passes have areas proportional to the radius of the system; consequently induction values B_{Mv} and B_{Lv} must be inversely proportional to this radius. We can therefore replace these inductions by the (constant) flux value:

$$\Delta\Phi_v = B(r)_v r\,\ell\Delta\alpha \qquad \ldots(8)$$

where ℓ is the length of the armature; B(r) can represent either the flux density in the magnet material or in the air-gap. Taking the thickness of the magnet as:

$$h = r_a - r_i \qquad \ldots(9)$$

and performing the integration, we obtain the equations:

$$\frac{\Delta\Phi_1}{\mu_0\mu_{rev}\,\ell\Delta\alpha}\ln\frac{r_a}{r_i} - \frac{B_{r1}}{\mu_0\mu_{rev}}h + \frac{\Delta\Phi_1}{\mu_0\,\ell\Delta\alpha}\ln\frac{r_i}{r_0} -$$
$$-\frac{\Delta\Phi_2}{\mu_0\mu_{rev}\,\ell\Delta\alpha}\ln\frac{r_a}{r_i} + \frac{B_{r2}}{\mu_0\mu_{rev}}h - \frac{\Delta\Phi_2}{\mu_0\,\ell\Delta\alpha}\ln\frac{r_i}{r_0} = NI\,, \qquad \ldots(10)$$

$$\frac{\Delta\Phi_1}{\mu_0\mu_{rev}\,\ell\Delta\alpha}\ln\frac{r_a}{r_i} - \frac{B_{r1}}{\mu_0\mu_{rev}}h + \frac{\Delta\Phi_1}{\mu_0\,\ell\Delta\alpha}\ln\frac{r_i}{r_0} -$$
$$-\frac{\Delta\Phi_3}{\mu_0\mu_{rev}\,\ell\Delta\alpha}\ln\frac{r_a}{r_i} + \frac{B_{r3}}{\mu_0\mu_{rev}}h - \frac{\Delta\Phi_3}{\mu_0\,\ell\Delta\alpha}\ln\frac{r_i}{r_0} = NI\,. \qquad \ldots(11)$$

At a distance of $\bar{r} = (r_i + r_0)/2$ from the system centre, (that is, half-way across the air-gap),

$$\Delta\Phi_v = B(\bar{r})_v \bar{r}\,\ell\Delta\alpha\,. \qquad \ldots(12)$$

Since we shall constantly be considering the value of B_v at this point let us put $B(\bar{r})_v \equiv B_v$. Eqs.(11) and (12) then become:

$$\frac{B_1\bar{r}}{\mu_0\mu_{rev}}\ln\frac{r_a}{r_i} - \frac{B_{r1}}{\mu_0\mu_{rev}}h + \frac{B_1\bar{r}}{\mu_0}\ln\frac{r_i}{r_0} - \frac{B_2\bar{r}}{\mu_0\mu_{rev}}\ln\frac{r_a}{r_i} +$$
$$+\frac{B_{r2}}{\mu_0\mu_{rev}}h - \frac{B_2\bar{r}}{\mu_0}\ln\frac{r_i}{r_0} = NI\,, \qquad \ldots(13)$$

$$\frac{B_1\bar{r}}{\mu_0\mu_{rev}}\ln\frac{r_a}{r_i} - \frac{B_{r1}}{\mu_0\mu_{rev}}h + \frac{B_1\bar{r}}{\mu_0}\ln\frac{r_i}{r_0} - \frac{B_3\bar{r}}{\mu_0\mu_{rev}}\ln\frac{r_a}{r_i} +$$
$$+\frac{B_{r3}}{\mu_0\mu_{rev}}h - \frac{B_3\bar{r}}{\mu_0}\ln\frac{r_i}{r_0} = NI\,, \qquad \ldots(14)$$

Or, if we introduce the abbreviations:

$$K = \frac{NI}{\dfrac{\bar{r}}{\mu_0}\left(\dfrac{1}{\mu_{rev}}\ln\dfrac{r_a}{r_i} + \ln\dfrac{r_i}{r_0}\right)}$$

and

$$A = \frac{h}{\bar{r}\left(\ln\dfrac{r_a}{r_i} + \mu_{rev}\ln\dfrac{r_i}{r_0}\right)}\,, \qquad \ldots(15)$$

the two equations can be written:

$$B_1 - B_2 = K + A(B_{r1} - B_{r2})\,, \qquad \ldots(16)$$

$$B_1 - B_3 = K + A(B_{r1} - B_{r3})\,. \qquad \ldots(17)$$

Let us express B_{rv} in the form of a general Fourier equation:

$$B_{rv} = B_r\sum b_n \sin n\phi\,. \qquad \ldots(18)$$

The coordinate system is chosen in such a way that no cosine terms can appear. This implies that the flux pattern will be asymmetrical at $\phi = 0$ and $\phi = 180°$.

Uniform magnetic potential prevails at the centre of the armature core, and also in the outer soft-iron ring. This means that for each flux path through pole-piece 1 (say), and through the air-gap and the adjoining portion of the permanent magnet, we can write:

$$\int_{r_i}^{r_a} H_{M1}dr + \int_{r_0}^{r_i} H_{L1}dr - \frac{2}{3}NI = \text{const.} \qquad \ldots(19)$$

Adopting the same procedure as above, we obtain*

$$B_1\left(\frac{\bar{r}}{\mu_0\mu_{rev}}\ln\frac{r_a}{r_i} + \frac{\bar{r}}{\mu_0}\ln\frac{r_i}{r_0}\right) = \frac{2}{3}NI + \text{const.} + \frac{B_{r1}}{\mu_0\mu_{rev}}h\,. \qquad \ldots(20)$$

This entitles us to set down the following general formula for B_v

$$B_v = a_v + AB_{rv}\,. \qquad \ldots(21)$$

It follows now from Eqs.(16) and (17) that,

$$a_1 - a_2 = K\,, \qquad \ldots(22)$$

$$a_1 - a_3 = K\,. \qquad \ldots(23)$$

Given the directions of magnetic induction shown in Fig. 3, and since the induction has a vanishing divergence (div B = 0), we can write:

$$\int_0^{2\pi}(B_1 + B_2 + B_3)d\phi = 0\,. \qquad \ldots(24)$$

The above equation carries the assumption that the developed torque is practically unaffected by induction values in those parts of the ring magnet which do not face any of the pole-pieces. It will be shown on page 207 that flux densities at these points are in fact very much smaller than in the air-gap.

Inserting Eqs.(21) and (18) in the above formula, we obtain:

$$\int_0^{2\pi}\Big[a_1 + a_2 + a_3 + AB_r\sum b_n \cdot$$
$$\cdot(\sin n\phi_1 + \sin n\phi_2 + \sin n\phi_3)\Big] = 0\,. \qquad \ldots(25)$$

If any point in pole-piece v is considered, ϕ_v is its angular displacement from the base-line and ϕ_{0v} is that of the centre of the pole-piece with respect to the base-line (see Fig. 3). The assumption referred to above implies that only those sectors of the angular system that encloses the pole pieces will contribute to the integral in Eq.(25); the sectors in question extend from $\phi_{0v} - \alpha$ to $\phi_{0v} + \alpha$, lying centrally about the axis of each pole-piece. Thus

$$(a_1 + a_2 + a_3)2\alpha - AB_r \cdot$$
$$\cdot\sum\frac{b_n}{n}\left(\cos n\phi_1\Big|_{\phi_{01}-\alpha}^{\phi_{01}+\alpha} + \cos n\phi_2\Big|_{\phi_{02}-\alpha}^{\phi_{02}+\alpha} + \right.$$
$$\left.+\cos n\phi_3\Big|_{\phi_{03}-\alpha}^{\phi_{03}+\alpha}\right) = (a_1 + a_2 + a_3)2\alpha + AB_r \cdot$$
$$\cdot\sum\frac{2b_n}{n}\sin n\alpha(\sin n\phi_{01} + \sin n\phi_{02} + \sin n\phi_{03}) = 0\,. \qquad \ldots(26)$$

We have still to take account of the fact that ϕ_{01}, ϕ_{02} and ϕ_{03} lie at 120° intervals; thus we obtain

$$(a_1 + a_2 + a_3)\alpha + AB_r\sum\frac{b_n}{n}\sin n\alpha \cdot$$
$$\cdot\left(1 + 2\cos\frac{2}{3}n\pi\right)\sin n\phi_{01} = 0\,, \qquad \ldots(27)$$

or:

$$a_1 + a_2 + a_3 = -3\frac{\delta}{\alpha}AB_r\sum\frac{b_n}{n}\sin n\alpha\sin n\phi_{01}\,, \qquad \ldots(28)$$

where δ has a value of unity for n = 3, 6, 9 and zero for all other whole-number values of n.* By introducing the abbreviation

$$Q = \frac{\delta}{\alpha}AB_r\sum\frac{b_n}{n}\sin n\alpha\sin n\phi_{01}\,, \qquad \ldots(29)$$

we can derive from Eqs.(22) and (23) the following system of equations:

$$\left.\begin{aligned} a_1 - a_2 &= K\,,\\ a_1 - a_3 &= K\,,\\ a_1 + a_2 + a_3 &= -3Q\,.\end{aligned}\right\} \qquad \ldots(30)$$

the roots of which are:

$$a_1 = \frac{2}{3}K - Q \quad a_2 = a_3 = -\frac{1}{3}K - Q\,. \qquad \ldots(31)$$

Inserting these values in Eq.(21), and taking account of Eq.(18), we get:

$$B_1 = \frac{2}{3}K - Q + AB_r\sum b_n\sin n\phi_1\,, \qquad \ldots(32)$$

$$B_2 = -\frac{1}{3}K - Q + AB_r\sum b_n\sin n\phi_2\,, \qquad \ldots(33)$$

$$B_3 = -\frac{1}{3}K - Q + AB_r\sum b_n\sin n\phi_3\,. \qquad \ldots(34)$$

At this point the calculations cannot be continued without knowledge of the energy in the air-gap, for it is from the changes of this energy with respect to time, that we shall have to derive the torque developed. This energy amounts to

$$E = \frac{1}{2}\int HBdV\,. \qquad \ldots(35)$$

Provided the air-gap width $s = r_i - r_0$ is small, the volume element can be defined as

$$dV = \ell\bar{r}sd\phi\,, \qquad \ldots(36)$$

where ℓ is the length of the armature. This yields the following expression for the torque developed:

$$M = \frac{dE_1}{d\phi_{01}} + \frac{dE_2}{d\phi_{02}} + \frac{dE_3}{d\phi_{03}} =$$
$$= \frac{1}{2}\frac{\ell\bar{r}s}{\mu_0}\frac{d}{d\phi_{01}}\int_0^{2\pi}(B_1^2 + B_2^2 + B_3^2)d\phi\,, \qquad \ldots(37)$$

where B_v again relates to the sectors enclosed by $\phi_{0v} - \alpha$ and $\phi_{0v} + \alpha$. The integral in the above equation has the value:

$$\int_0^{2\pi}(B_1^2 + B_2^2 + B_3^2)d\phi =$$
$$= \int_0^{2\pi}\Big[\frac{2}{3}K^2 + 3Q^2 + 2AB_r\left(\frac{2}{3}K - Q\right)\sum b_n\sin n\phi_1 -$$
$$-2AB_r\left(\frac{1}{3}K + Q\right)\sum b_n\sin n\phi_2 -$$
$$-2AB_r\left(\frac{1}{3}K + Q\right)\sum b_n\sin n\phi_3 +$$
$$+A^2B_r^2\Big(\sum\sum b_nb_m\sin n\phi_1\sin m\phi_1 +$$
$$+\sum\sum b_nb_m\sin n\phi_2\sin m\phi_2 +$$
$$+\sum\sum b_nb_m\sin n\phi_3\sin m\phi_3\Big)\Big]d\phi =$$
$$= \frac{4}{3}K^2\alpha + 6\alpha Q^2 -$$
$$-2AB_r\left(\frac{2}{3}K - Q\right)\sum\frac{b_n}{n}\cos n\phi_1\Big|_{\phi_{01}-\alpha}^{\phi_{01}+\alpha} +$$
$$+2AB_r\left(\frac{1}{3}K + Q\right)\sum\frac{b_n}{n}\cos n\phi_2\Big|_{\phi_{02}-\alpha}^{\phi_{02}+\alpha} +$$
$$+2AB_r\left(\frac{1}{3}K + Q\right)\sum\frac{b_n}{n}\cos n\phi_3\Big|_{\phi_{03}-\alpha}^{\phi_{03}+\alpha} +$$
$$+A^2B_r^2\sum\sum b_nb_m\Big\{\Big[\frac{1}{2(n-m)}\sin(n-m)\phi_1 -$$
$$-\frac{1}{2(n+m)}\sin(n+m)\phi_1\Big]\Big|_{\phi_{01}-\alpha}^{\phi_{01}+\alpha} +$$
$$+\Big[\frac{1}{2(n-m)}\sin(n-m)\phi_2 -$$
$$-\frac{1}{2(n+m)}\sin(n+m)\phi_2\Big]\Big|_{\phi_{02}-\alpha}^{\phi_{02}+\alpha} +$$
$$+\Big[\frac{1}{2(n-m)}\sin(n-m)\phi_3 -$$
$$-\frac{1}{2(n+m)}\sin(n+m)\phi_3\Big]\Big|_{\phi_{03}-\alpha}^{\phi_{03}+\alpha}\Big\} =$$
$$= \frac{4}{3}K^2\alpha + 6\alpha Q^2 +$$
$$+4AB_r\left(\frac{2}{3}K - Q\right)\sum\frac{b_n}{n}\sin n\alpha\sin n\phi_{01} -$$
$$-4AB_r\left(\frac{1}{3}K + Q\right)\sum\frac{b_n}{n}\sin n\alpha\sin n\phi_{02} -$$
$$-4AB_r\left(\frac{1}{3}K + Q\right)\sum\frac{b_n}{n}\sin n\alpha\sin n\phi_{03} +$$
$$+A^2B_r^2\sum\sum b_nb_m.\Big\{\frac{\sin(n-m)\alpha}{n-m}\cos(n-m)\phi_{01} -$$
$$-\frac{\sin(n+m)\alpha}{n+m}\cos(n+m)\phi_{01} +$$
$$+\frac{\sin(n-m)\alpha}{n-m}\cos(n-m)\phi_{02} -$$

---

*It can further be seen from this equation that, provided the air-gap is sufficiently small compared to r_i or r_0, the flux density B_v in the air-gap may have a higher value than is indicated by the intersection of the demagnetisation curve by the ordinate, even when no current is flowing through the armature windings.

*The even harmonics will not be considered in the present treatment because they create an asymmetric flux distribution at $\phi = \pi/2$ and $\phi = 3\pi/2$.

$$\begin{aligned}&-\frac{\sin(n+m)\alpha}{n+m}\cos(n+m)\phi_{02}+\\&+\frac{\sin(n-m)\alpha}{n-m}\cos(n-m)\phi_{03}-\\&-\frac{\sin(n+m)\alpha}{n+m}\cos(n+m)\phi_{03}\Big\}.\end{aligned} \qquad \ldots(38)$$

If we again make use of the fact that ϕ_{01}, ϕ_{02} and ϕ_{03} lie at 120° intervals we can reduce the foregoing to:

$$\begin{aligned}\int_0^{2\pi}(B_1{}^2+B_2{}^2+B_3{}^2)d\phi &= \frac{4}{3}K^2\alpha+6\alpha Q^2-\\&-4AB_rQ\sum\frac{b_n}{n}\sin n\alpha\left(1+2\cos\frac{2}{3}n\pi\right)\sin n\phi_{01}+\\&+\frac{8}{3}AB_rK\sum\frac{b_n}{n}\sin n\alpha\left(1-\cos\frac{2}{3}n\pi\right)\sin n\phi_{01}+\\&+A^2B_r{}^2\sum\sum b_nb_m\cdot\\&\cdot\left\{\frac{\sin(n-m)\alpha}{n-m}\left[1+2\cos(n-m)\frac{2\pi}{3}\right]\cos(n-m)\phi_{01}-\right.\\&\left.-\frac{\sin(n+m)\alpha}{n+m}\left[1+2\cos(n+m)\frac{2\pi}{3}\right]\cos(n+m)\phi_{01}\right\}.\end{aligned} \qquad \ldots(39)$$

Reference to Eq.(29) will reveal that the third term of the above expression has the value $-12\alpha Q^2$. Inserting this in Eq.(37), and differentiating, we obtain the following for torque M_a

$$\begin{aligned}M_a = {}&\frac{4}{3}\frac{\ell\bar{r}s}{\mu_0}AB_rK\cdot\\&\cdot\sum b_n\sin n\alpha\left(1-\cos\frac{2}{3}n\pi\right)\cos n\phi_{01}-\\&-\frac{1}{2}\frac{\ell\bar{r}s}{\mu_0}A^2B_r{}^2\sum\sum b_nb_m\cdot\\&\cdot\left\{\sin(n-m)\alpha\left[1+2\cos(n-m)\frac{2\pi}{3}\right]\sin(n-m)\phi_{01}-\right.\\&\left.-\sin(n+m)\alpha\left[1+2\cos(n+m)\frac{2\pi}{3}\right]\sin(n+m)\phi_{01}\right\}-\\&-6\frac{\ell\bar{r}s}{\alpha\mu_0}A^2B_r{}^2\delta_{nm}\sum\sum\frac{b_nb_m}{n}\cdot\\&\cdot\sin n\alpha\sin m\alpha\sin n\phi_{01}\cos m\phi_{01}.\end{aligned} \qquad \ldots(40)$$

The index α indicates that the torque value given by the above expression is that appropriate to the armature position shown in Fig. 2(a). The symbol δ_{mn} in the last term of the equation is intended to convey that the term vanishes except when both n and m have values in the series 3, 9, 15...

If we take account of the 3rd, 5th, and 7th harmonics in addition to the fundamental (no account need be taken of even harmonics; see the footnote on page 203) we obtain the following expression for the torque

$$\begin{aligned}M_a = {}&2\frac{\ell\bar{r}s}{\mu_0}AB_rK(b_1\sin\alpha\cos\phi_{01}+b_5\sin5\alpha\cos5\phi_{01}+\\&+b_7\sin7\alpha\cos7\phi_{01})+\\&+\frac{\ell\bar{r}s}{\mu_0}A^2B_r{}^2b_3{}^2\left(\frac{3}{2}\sin6\alpha-\frac{\sin^23\alpha}{\alpha}\right)\sin6\phi_{01}+\\&+3\frac{\ell\bar{r}s}{\mu_0}A^2B_r{}^2\Big[b_1(b_5-b_7)\sin6\alpha\sin6\phi_{01}+\\&+b_5b_7\sin12\alpha\sin12\phi_{01}\Big].\end{aligned} \qquad \ldots(41a)$$

The first summand in the above expression represents the useful torque, which is dependent on current; the second and third summands represent permanent-magnetic pole sensitivity. Eq.(41a) has been derived in respect of the armature position and the form of magnetisation as shown in diagram (a) of Fig. 2. All that is necessary, to deduce the torque in other armature positions, is to rotate the angle ϕ_{01} through 60°, 120°, 180° and so on; that is, to insert $\phi_{01}-\pi/3$, $\phi_{01}-2\pi/3$, $\phi_{01}-\pi$ into Eq.(41a).

For example, for the armature position shown in diagram (b) of Fig. 2, we obtain,

$$\begin{aligned}M_b = {}&\frac{\ell\bar{r}s}{\mu_0}AB_rK[b_1\sin\alpha(\cos\phi_{01}+\sqrt{3}\sin\phi_{01})+\\&+b_5\sin5\alpha(\cos5\phi_{01}-\sqrt{3}\sin5\phi_{01})+\\&+b_7\sin7\alpha(\cos7\phi_{01}+\sqrt{3}\sin7\phi_{01})]+\\&+\frac{\ell\bar{r}s}{\mu_0}A^2B_r{}^2b_3{}^2\left(\frac{3}{2}\sin6\alpha-\frac{\sin^23\alpha}{\alpha}\right)\sin6\phi_{01}+\\&+3\frac{\ell\bar{r}s}{\mu_0}A^2B_r{}^2[b_1(b_5-b_7)\sin6\alpha\sin6\phi_{01}+\\&+b_5b_7\sin12\alpha\sin12\phi_{01}].\end{aligned} \qquad \ldots(41b)$$

Inspection of the above will reveal that only the first summand of Eq.(41a) has changed, while the second and third, representing permanent-magnetic pole sensitivity, are the same. For the torque developed at the armature positions as shown in diagrams (c) ... (f), we need only write down those components which are dependent on current, and which we will denote as M':

$$\begin{aligned}M_c{}' = {}&\frac{\ell\bar{r}s}{\mu_0}AB_rK[b_1\sin\alpha(-\cos\phi_{01}+\sqrt{3}\sin\phi_{01})+\\&+b_5\sin5\alpha(-\cos5\phi_{01}-\sqrt{3}\sin5\phi_{01})+\\&+b_7\sin7\alpha(-\cos7\phi_{01}+\sqrt{3}\sin7\phi_{01})],\end{aligned} \qquad \ldots(41c)$$

$$\begin{aligned}M_d{}' = {}&2\frac{\ell\bar{r}s}{\mu_0}AB_rK(-b_1\sin\alpha\cos\phi_{01}-\\&-b_5\sin5\alpha\cos5\phi_{01}-b_7\sin7\alpha\cos7\phi_{01}),\end{aligned} \qquad \ldots(41d)$$

$$\begin{aligned}M_e{}' = {}&\frac{\ell\bar{r}s}{\mu_0}AB_rK[b_1\sin\alpha(-\cos\phi_{01}-\sqrt{3}\sin\phi_{01})+\\&+b_5\sin5\alpha(-\cos5\phi_{01}+\sqrt{3}\sin5\phi_{01})+\\&+b_7\sin7\alpha(-\cos7\phi_{01}-\sqrt{3}\sin7\phi_{01})],\end{aligned} \qquad \ldots(41e)$$

$$\begin{aligned}M_f{}' = {}&\frac{\ell\bar{r}s}{\mu_0}AB_rK[b_1\sin\alpha(\cos\phi_{01}-\sqrt{3}\sin\phi_{01})+\\&+b_5\sin5\alpha(\cos5\phi_{01}+\sqrt{3}\sin5\phi_{01})+\\&+b_7\sin7\alpha(\cos7\phi_{01}-\sqrt{3}\sin7\phi_{01})].\end{aligned} \qquad \ldots(41f)$$

On plotting these current-dependent components of torque against ϕ_{01} considering the fundamental only, the wave pattern shown in Fig. 4 is obtained: it consists of six individual ripples with peaks at $\phi = 0°, 60°, 120°$ and so on, and minima, occurring at 30°, 90°, 150° and so on, having a value which is $\sqrt{3}/2$ that of the maxima.

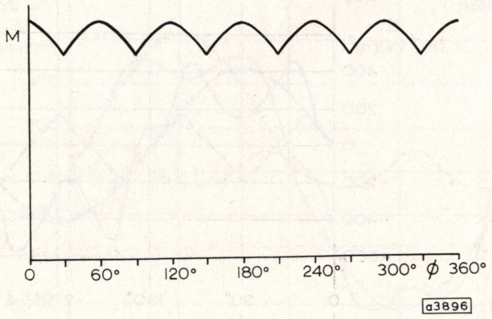

Fig. 4—Torque due to flux linkage

The mean torque developed can be obtained by integrating over a single ripple; namely, from −30° to 30°(M_a) say, or from 30° to 90°(M_b). The same value is found for each ripple: it is,

$$\bar{M} = \frac{3}{\pi}\int_{-\pi/6}^{+\pi/6}M_ad\phi_{01} = \frac{3}{\pi}\int_{+\pi/6}^{+\pi/2}M_bd\phi_{01} = \frac{6}{\pi}\frac{\ell\bar{r}s}{\mu_0}AB_rK\cdot\left(b_1\sin\alpha+\frac{b_5}{5}\sin5\alpha-\frac{b_7}{7}\sin7\alpha\right). \qquad \ldots(42)$$

Those components of M that represent permanent-magnetic pole sensitivity have no effect on $\bar{M}$. This pole sensitivity does not in fact interfere with the operation of the motor or modify its characteristic; it merely causes the motor to run with a certain degree of unevenness.

From the calculations carried out so far the following conclusions can be drawn.

1. The torque acting on the armature, in so far as it is due to the armature's current, is dependent on the fundamental of the magnetic induction and on its 5th and 7th harmonics, but not on its 3rd harmonic.
2. This implies that an electromagnetic pole sensitivity must always be present; indeed, it can never be ignored since the 3rd harmonic (as also the 9th, 15th, 21st and so on) makes no contribution to the first term of Eq.(41).
3. The total harmonics contribute to permanent-magnetic pole sensitivity.
4. The third harmonic represents a rather special case in this connection: at small values of α, the two bracketed expressions in the second term of Eq.(41) almost cancel each other out (see Fig. 5). The term attains a maximum at $\alpha = 39°$, thereafter falling off. Other harmonics with threefold symmetry ($n = 9$, 15, 21 ...) are subject to a similar kind of compensation effect. For this reason, and because the b_n coefficients generally form a zero series, it is always possible to disregard the influence of the terms in question. Terms involving coefficients of the form $b_1b_3\beta$ never occur, as can readily be seen from the second term of Eq.(40).

It would be wrong, however, to infer from conclusions 1 and 3 that the 3rd harmonic has only undesirable effects, and should therefore be eliminated. It is possible to contrive, by adding a 3rd harmonic of suitable amplitude to the fundamental, to ensure that B_{rv} (see Eq.18) nowhere exceeds the remanence B_r of the magnet material, even though the amplitude of the fundamental may be greater than B_r; that is, $b_1>1$. In this way, the 3rd harmonic allows a higher torque to be obtained than is possible with the fundamental alone, and the electromagnetic pole sensitivity remains unchanged. We need not consider the 5th and 7th harmonics here because the increase in torque they afford is not large, whereas the increase in pole sensitivity they entail may be quite considerable.

The object of the calculations which follow is to determine the angle at which B_{rv} attains the remanence value B_r in the case of fundamental plus 3rd harmonic, and also to evaluate coefficients b_1 and b_3.

The extreme values of B_{rv} can be obtained by differentiating:

$$B_{rv} = B_r(b_1\sin\phi+b_3\sin3\phi), \qquad \ldots(43)$$

$$\frac{dB_{rv}}{d\phi} = B_r(b_1\cos\phi+3b_3\cos3\phi) = 0. \qquad \ldots(44)$$

We find that the minima occur at:

$$\cos\phi = 0, \qquad \ldots(45a)$$

and the maxima at:

$$\sin\phi = \sqrt{\frac{b_1+3b_3}{12b_3}}. \qquad \ldots(45b)$$

At these angles where the maxima are attained, $B_{rv} = Br$, and hence also,

$$b_1\sin\phi+b_3\sin3\phi = 1. \qquad \ldots(46)$$

Insertion in the above of Eq.(45b) yields a relation connecting b_1 and b_3:

$$b_1 = 3(\sqrt[3]{b_3}-b_3). \qquad \ldots(47)$$

If a high torque is to be obtained, b_1 must be as large as possible; it is required, then, that,

$$\frac{db_1}{db_3} = 0. \qquad \ldots(48)$$

From these last two equations b_1 and b_3 are evaluated

$$b_1 = \frac{2}{\sqrt{3}} = 1{\cdot}155\ ;\ b_3 = \frac{1}{3\sqrt{3}} = 0{\cdot}1925. \qquad \ldots(49)$$

Finally, on inserting these values in Eq.(45b) we arrive at the angles at which $B_{rv} = B_r$:

$$\phi = 60°, 120°, 240°, \text{and } 300°$$

The total torque developed now becomes

$$M_a = \frac{4}{\sqrt{3}}\frac{\ell\bar{r}s}{\mu_0}AB_rK\sin\alpha\cos\phi_{01}+\frac{1}{27}\frac{\ell\bar{r}s}{\mu_0}A^2B_r{}^2\cdot\left(\frac{3}{2}\sin6\alpha-\frac{\sin^23\alpha}{\alpha}\right)\sin6\phi_{01}. \qquad \ldots(50)$$

Adding the 3rd harmonic thus has the effect of increasing by about 15% the torque obtained from a system that has undergone purely sinusoidal magnetisation, though

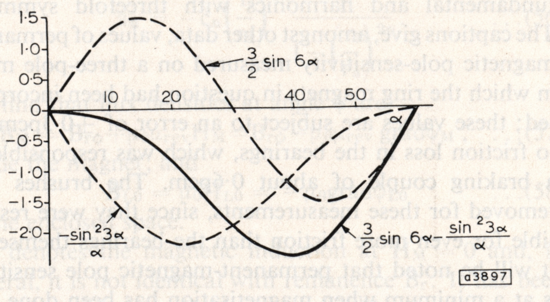

Fig. 5—Analysis of third harmonic

in some circumstances it may mean that a certain small degree of permanent-magnetic pole sensitivity must also be accepted. On the other hand, if magnetisation is done with a square wave, so that,

$$B_{rv} = B_r \frac{4}{\pi} \sum \frac{\sin n\phi}{n},$$

then $\bar{M}$, the torque due to the fundamental, will be greater by a factor of $4/\pi$, and the 5th and 7th harmonics will together provide a further gain of about 5% (for $\alpha = 30°$), the contribution of the other harmonics being less than 1%. Therefore square-wave magnetisation provides approximately a 34% gain in torque, but naturally entails a high degree of pole sensitivity as well.

It is assumed in the above calculations that the armature is of the same length ℓ as the ring magnet. If the armature is made slightly shorter than the magnet, then the torque will not be reduced in the same proportion: the lines of force issuing from the ring magnet at points that now have no armature iron in front of them are nevertheless attracted toward the armature, and enter its material. Thus a shortening of the armature length ℓ increases the flux density in the armature iron. The air-gap volume is now somewhat larger than that over which integration was performed in Eq.(37); consequently, the torque developed is somewhat greater than is to be expected from Eq.(41) above.

Thus the lines of force entering other faces of the armature pole-pieces are similarly affected, the net result being an increase in the effective value of α, and, in general, a developed torque that is higher than the calculated value.

Motor Measurements

In order to get an experimental check on the calculations carried out in the preceding section, ring magnets made of Magnadur 1, of dimensions $r_a = 1{\cdot}075$cm, $r_i = 0{\cdot}8$cm and $\ell = 1{\cdot}2$cm, were subjected to different magnetising processes. Figs. 6 to 10 show the flux densities obtained from these Magnadur rings, the curves of $B_{L(\phi)}$ being in solid line. The sinusoidal chain-dotted curves represent the fundamental, the broken-line curves the sum of harmonics with threefold symmetry ($n = 3, 9, 15\ldots$). At the bottom of each graph, plotted on the same scale, is a curve obtained by subtracting the relevant fundamental and three-fold harmonics from the curve obtained by plotting measured induction values.

These resultant values are comparatively large in the cases represented by Figs. 6 to 8, but the magnetisation processes to which Figs. 9 and 10 refer result in $B_{L(\Phi)}$ curves which can be almost completely resolved into a fundamental and harmonics with threefold symmetry. The captions give, amongst other data, values of permanent-magnetic pole-sensitivity measured on a three-pole motor in which the ring magnets in question had been incorporated; these values are subject to an error of ±0·3pcm due to friction loss in the bearings, which was responsible for a braking couple of about 0·6pcm. The brushes were removed for these measurements, since they were responsible for even more friction than the bearings themselves. It will be noted that permanent-magnetic pole sensitivity is at a minimum when magnetisation has been done with the fundamental alone, or practically alone (Fig. 9).

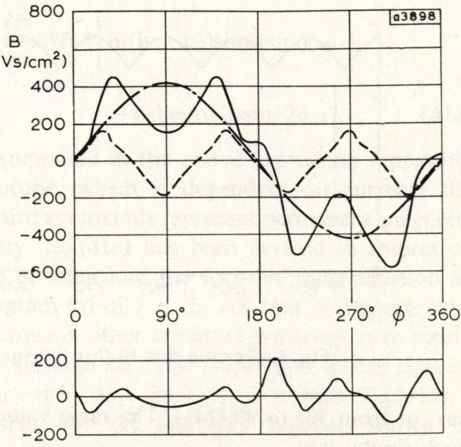

Fig. 6

Figs. 6 to 10—Flux densities in air-gap of five miniature d.c. motors

	Permanent-magnetic pole sensitivity (pcm)	Starting voltage (V)
Fig. 6	5·1	0·93
Fig. 7	7·8	1·26
Fig. 8	6·1	1·02
Fig. 9	0·3	0·69
Fig. 10	0·9	0·71

When a fairly high-amplitude 3rd harmonic is added (Fig. 10), pole sensitivity is still a good deal less than the values measured in the cases to which Figs. 6 to 8 relate, as is shown by the amplitudes of the curves in the lower part of the relevant graphs. In fact, the measurements tend to support the theory set up in the preceding section.

Furthermore, the current I_K through the unloaded motor at start-up varies in much the same way as the pole sensitivity, because the torque as given by Eq.(41) is directly proportional to the motor current, and Eq.(1) shows that the greater the pole sensitivity M_P, the greater must be the torque M_{K0} created by the short-circuit current. Clearly, then, so long as the braking couple M_R remains the same, high pole sensitivity will always be associated with a heavy starting current I_K, and vice versa. The captions to Figs. 6 to 10 also specify the starting voltages across the unloaded armatures, which are naturally proportional to the starting currents. They are all measured values, obtained from the same armature and commutator assembly, but with different field magnets in regard to the magnetisation process utilised. 'Starting' voltage is a composite quantity, made up of the voltage drop across the ohmic resistance of the armature winding plus any contact drops at the commutator. This fact, and the need to allow for commutator friction, admittedly detracts from the reliability of the measurements. The starting voltage of battery-operated devices can often be taken as a measure of the least allowable power provided by the battery. Clearly, there is a definite interdependence between starting voltage and pole sensitivity, despite the uncertainties referred to above, which are naturally of some importance in the small motors being dealt with.

Relationship between Flux Densities Prevailing in the Presence and Absence of an Armature

As a general rule, radial magnetisation is carried out

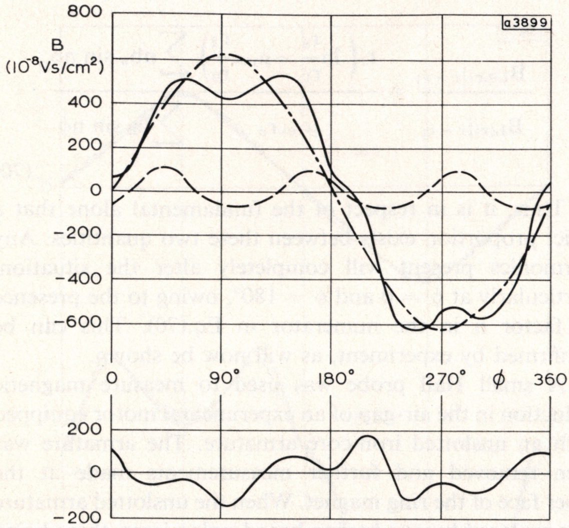

Fig. 7

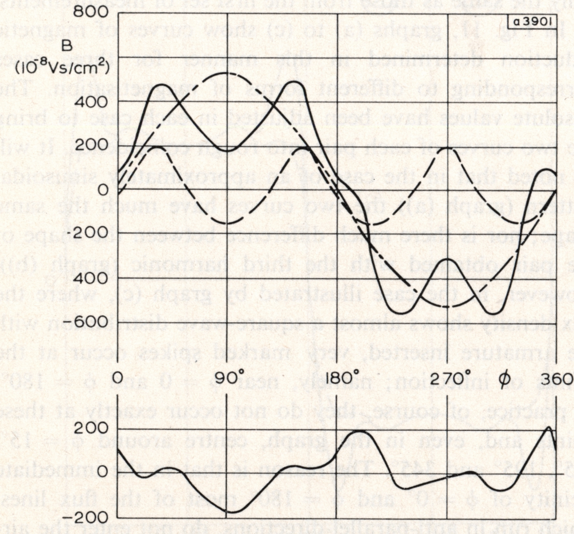

Fig. 8

before the motor is assembled, and in any case before the armature is inserted. This presents no problems at all when the field magnets are of Magnadur 1 or 3 (improved version), materials which have demagnetisation characteristics that are linear over a very wide range. In the case of radial magnetisation it is important to know how the radial components of the magnetic induction alter when the armature is inserted. In order to find out something about the relationship between induction values in the absence and the presence of the armature, we shall start by considering the system minus-armature. The following general expression can be written for the magnetic potential in the ring or segments:

$$\psi_M = \psi_0 \sum a_n \left[\left(\frac{r}{r_a}\right)^n - \left(\frac{r}{r_a}\right)^{-n}\right] \sin n\phi. \quad \ldots(51)$$

A similar expression for the magnetic potential in the space enclosed by the ring magnet (in air, and in the absence of an armature) is:

$$\psi_{L0} = \psi_0 \sum c_n \left(\frac{r}{r_a}\right)^n \sin n\phi. \quad \ldots(52)$$

These are the roots of the potential equation, and they

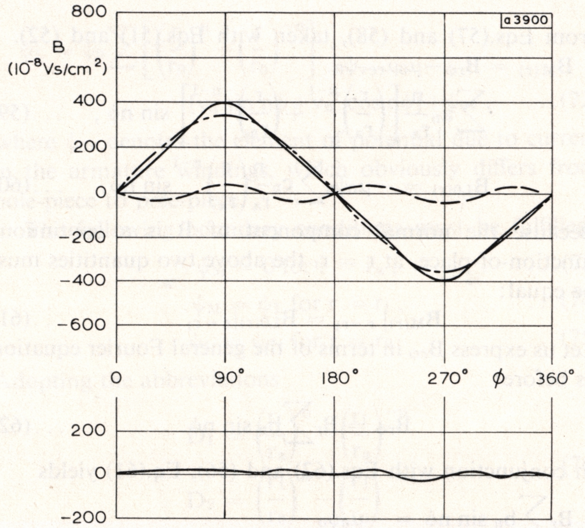

Fig. 9

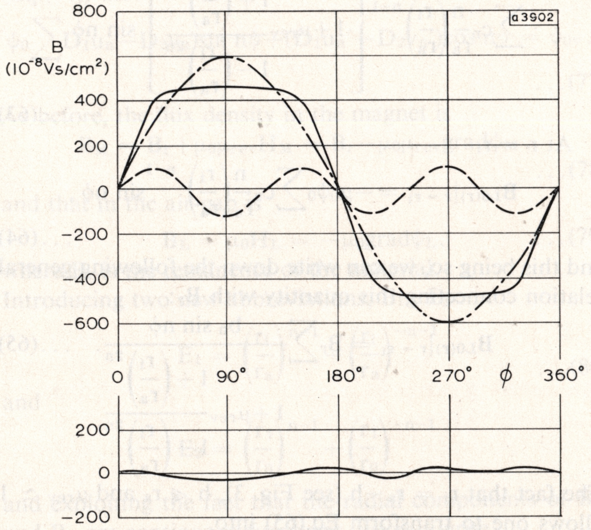

Fig. 10

also enable the following boundary conditions to be fulfilled:

$$\psi_M = 0 \begin{cases} \text{for } r = r_a\,, \\ \text{for } \phi = 0,\ \phi = \pi\,, \end{cases} \quad \ldots(53)$$

$$\psi_M = \psi_{L0} \text{ for } r = r_i\,, \quad \ldots(54)$$

$$\psi_{L0} = 0 \begin{cases} \text{for } r = 0\,, \\ \text{for } \phi = 0,\ \phi = \pi. \end{cases} \quad \ldots(55)$$

The second condition (Eq.54) implies that

$$a_n = -c_n \left(\frac{r_i}{r_a}\right)^{2n} \frac{1}{1-\left(\frac{r_i}{r_a}\right)^{2n}}. \quad \ldots(56)$$

We find that flux densities at angle ϕ are,

$$B_M = B_{r\phi} + \mu_0\mu_{rev}H_M = B_{r\phi} - \mu_0\mu_{rev}\,\text{grad}\psi_M\,, \quad \ldots(57)$$

inside the magnet; and

$$B_{L0} = \mu_0 H_{L0} = -\mu_0 \text{grad}\psi_{L0} \quad \ldots(58)$$

in the enclosed space.

$B_r\phi$ denotes the magnetic induction at $H_M = 0$ and, in general, it is not identical with remanence B_r. It has been assumed to have a radial component only. On the strength of this, we can derive radial components $B_{M(r)}$ and $B_{L(r)}$

from Eqs.(57) and (58), taken with Eqs.(51) and (52).

$$B_{M(r)} = B_{r\phi} - \mu_0\mu_{rev}\psi_0 \cdot \sum a_n \frac{n}{r_a}\left[\left(\frac{r}{r_a}\right)^{n-1} + \left(\frac{r}{r_a}\right)^{-n-1}\right] \sin n\phi\,, \qquad \ldots(59)$$

$$B_{L0(r)} = -\mu_0\psi_0 \sum c_n \frac{n}{r_a}\left(\frac{r}{r_a}\right)^{n-1} \sin n\phi\,. \qquad \ldots(60)$$

Because the normal component of B is a continuous function-of-place, at $r = r_i$ the above two quantities must be equal:

$$B_{M(r)}\big|_{r=r_i} = B_{L0(r)}\big|_{r=r_i}\,. \qquad \ldots(61)$$

Let us express $B_{r\phi}$ in terms of the general Fourier equation as before:

$$B_{r\phi} = B_r \sum b_n \sin n\phi\,. \qquad \ldots(62)$$

In conjunction with Eqs.(62) and (56), Eq.(61) yields

$$B_r \sum b_n \sin n\phi = -\mu_0\psi_0 \cdot \sum c_n \frac{n}{r_a}\left(\frac{r_i}{r_a}\right)^{n-1}\left[1 + \mu_{rev}\frac{1+\left(\dfrac{r_i}{r_a}\right)^{2n}}{1-\left(\dfrac{r_i}{r_a}\right)^{2n}}\right] \sin n\phi\,. \qquad \ldots(63)$$

At $r = r_i$

$$B_{L0(r)}\big|_{r=r_i} = -\mu_0\psi_0 \sum c_n \frac{n}{r_a}\left(\frac{r_i}{r_a}\right)^{n-1} \sin n\phi\,, \qquad \ldots(64)$$

and this being so, we can write down the following general relation connecting this quantity with B_r:

$$B_{L0(r)}\big|_{r=r_i} = B_r \sum \frac{b_n \sin n\phi}{1 + \mu_{rev}\dfrac{1+\left(\dfrac{r_i}{r_a}\right)^{2n}}{1-\left(\dfrac{r_i}{r_a}\right)^{2n}}}\,. \qquad \ldots(65)$$

The fact that $r_i = r_a - h$ (see Fig. 3), $h \ll r_a$ and $\mu_{rev} \simeq 1$ allows one to transform Eq.(65) into,

$$B_{L0(r)}\big|_{r=r_i} = B_r \frac{h}{\mu_{rev} r_\alpha} \sum n b_n \sin n\phi\,. \qquad \ldots(66)$$

Let us now suppose that the armature has been inserted, and that no current is flowing through its windings; the flux density $B_{L(r)}$ now prevailing at $r = r_i$ can easily be expressed as a function of remanence B_r:

$$\int_{r_i}^{r_a} H_M dr + \int_{r_0}^{r_i} H_L dr = 0\,. \qquad \ldots(67)$$

Because Magnadur 1 has a linear demagnetisation characteristic we can again make use of the relation:

$$H_M = \frac{B_M - B_{r\phi}}{\mu_0\mu_{rev}}\,. \qquad \ldots(68)$$

Adopting the same procedure as was employed to derive Eqs.(5) to (14) we find that:

$$B_{L(r)}\big|_{r=r_i} = \frac{B_{r\phi} h}{r_i\left(\ln\dfrac{r_a}{r_i} + \mu_{rev}\ln\dfrac{r_i}{r_0}\right)}\,. \qquad \ldots(69)$$

We can now deduce from Eqs.(66) and (69), taking account of Eq.(62), a straightforward relationship between the two radial components of the flux densities at $r = r_i$ in the air-gap:

$$\frac{B_{L0(r)}\big|_{r=r_i}}{B_{L(r)}\big|_{r=r_i}} = \frac{r_i\left(\ln\dfrac{r_a}{r_i} + \mu_{rev}\dfrac{r_i}{r_0}\right)}{\mu_{rev} r_a} \, \frac{\sum n b_n \sin n\phi}{\sum b_n \sin n\phi}\,. \qquad \ldots(70)$$

Thus, it is in respect of the fundamental alone that a strict proportion exists between these two quantities. Any harmonics present will completely alter the situation, particularly at $\phi = 0$ and $\phi = 180°$, owing to the presence of factor n in the numerator in Eq.(70). This can be confirmed by experiment, as will now be shown.

A small Hall probe was used to measure magnetic induction in the air-gap of an experimental motor equipped with an unslotted iron-core armature. The armature was then removed and further measurements made at the inner face of the ring magnet. When the unslotted armature was replaced by one having broad pole-pieces, these being rotated in stages, results were obtained that were practically the same as those from the first set of measurements.

In Fig. 11, graphs (a) to (c) show curves of magnetic induction determined in this manner for three cases corresponding to different forms of magnetisation. The absolute values have been adjusted in each case to bring the two curves of each pair into rough coincidence. It will be noted that in the case of an approximately sinusoidal pattern (graph (a)) the two curves have much the same shape; nor is there much difference between the shape of the pair obtained with the third harmonic (graph (b)). However, in the case illustrated by graph (c), where the flux density shows almost a square-wave distribution with the armature inserted, very marked spikes occur at the points of inflection; namely, near $\phi = 0$ and $\phi = 180°$. In practice, of course, they do not occur exactly at these points and, even in the graph, centre around $\phi = 15°$, 165°, 195° and 345°. The reason is that in the immediate vicinity of $\phi = 0°$ and $\phi = 180°$ most of the flux lines, which run in anti-parallel directions, do not enter the air-gap but close back on themselves inside the magnetic material.

The measurements just referred to represent some confirmation of the theory put forward above, and of Eq.(70) in particular. The relationships demonstrated in this section of the article must always be borne in mind when radial magnetisation is undertaken: It is usual, of course, to carry out the process before the motor is assembled.

TRANSVERSE MAGNETISATION

Calculation of Torque

For many types of small d.c. motor it can be advantageous to choose a magnetisation process other than that so far considered, and known as diametric or transverse magnetisation; the resulting induction lines, in a model with an unslotted armature, are shown schematically in Fig. 12. A good approximation to this flux pattern is possible in practice; and it is the only one which, at the present time, can be conferred, without undue difficulty, on the finished assembly – that is, the complete motor with its housing, armature, gearing, and so on.

In a transversely-magnetised system the magnet thickness, h, is a function of ϕ, which means that any attempt to adopt the procedure employed on page 201 for calculating the torque will meet with considerable difficulties. The problem can, however, be resolved by 'potential theory', and by assuming in the first place that every part of the magnet has a working point on the extreme demagnetisation curve of the material. The following general equation can be written for the magnetic potential inside the material:

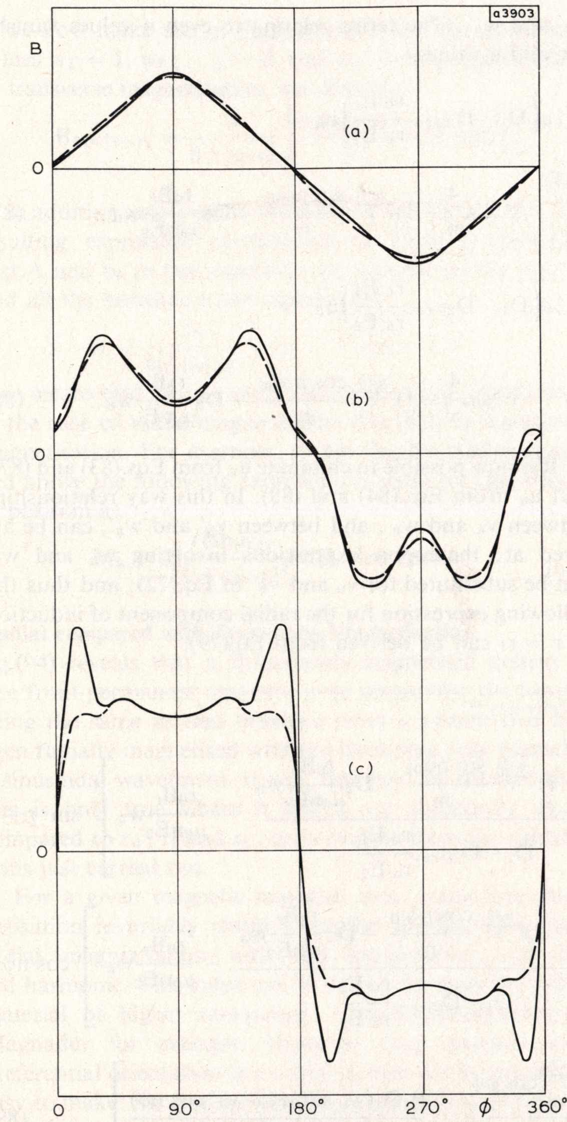

Fig. 11—Flux densities in three experimental motors
——— at surface of ring magnet in open system minus armature
- - - - - - in air-gap between ring magnet and unslotted armature

$$\psi_M = \psi_0 \sum \left[\left(\frac{r}{r_a}\right)^{n} - \left(\frac{r}{r_a}\right)^{-n}\right] \cdot [u_n \sin n\phi + u_n' \cos n\phi]\,, \qquad \ldots(71)$$

For the time being we are including terms with even values of n, and considering ϕ in the region lying between $\phi_{0v} - \alpha$ and $\phi_{0v} + \alpha$. The magnetic potential in the air-gap is:

$$\psi_L = \psi_0 \sum \left[\left(\frac{r}{r_0}\right)^{n} - \left(\frac{r}{r_0}\right)^{-n}\right] \cdot [v_n \sin n\phi + v_n' \cos n\phi] + \psi_{0v}\,, \qquad \ldots(72)$$

where ψ_{0v} denotes the element of potential due to current in the armature windings, which obviously differs from pole-piece to pole-piece.

The following boundary conditions must be fulfilled:

$$\psi_M = 0 \text{ for } r = r_a\,, \qquad \ldots(73)$$

$$\psi_M = \psi_L \text{ for } r = r_i\,, \qquad \ldots(74)$$

$$\psi_L = \psi_{0v} \text{ for } r = r_0\,. \qquad \ldots(75)$$

Adopting the abbreviations

$$D_1 = \left(\frac{r_i}{r_a}\right)^{n} - \left(\frac{r_i}{r_a}\right)^{-n} \qquad D_2 = \left(\frac{r_i}{r_0}\right)^{n} - \left(\frac{r_i}{r_0}\right)^{-n} \qquad \ldots(76)$$

we must infer from the second of these conditions (Eq.(74)) that

$$\psi_0 \sum D_1 u_n - D_2 v_n) \sin n\phi + (D_1 u_n' - D_2 v_n') \cos n\phi = \psi_{0v}\,. \qquad \ldots(77)$$

As before, the flux density in the magnet is

$$B_M = B_r + \mu_0\mu_{rev} H_M = B_r - \mu_0\mu_{rev} \,\mathrm{grad}\,\psi_M\,, \qquad \ldots(78)$$

and that in the air-gap is

$$B_L = \mu_0 H_L = -\mu_0 \,\mathrm{grad}\,\psi_L\,. \qquad \ldots(79)$$

where B_r is the remanence of the material.

Introducing two new abbreviations, E_1, E_2:

$$E_1 = \left(\frac{r_i}{r_a}\right)^{n-1} + \left(\frac{r_i}{r_a}\right)^{-n-1} \qquad \ldots(80)$$

and

$$E_2 = \left(\frac{r_i}{r_0}\right)^{n-1} + \left(\frac{r_i}{r_0}\right)^{-n-1}$$

and exploiting the fact that the radial components of B_M and B_L are continuous functions, we can write

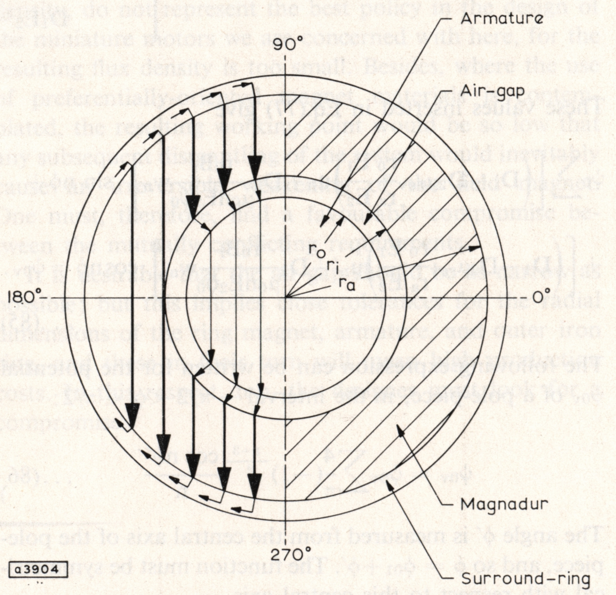

Fig. 12—Lines of induction in transversely-magnetised motor with unslotted armature

$$\frac{B_{r(r)}}{\mu_0} - \mu_{rev}\psi_0 \sum \frac{n}{r_a} E_1 (u_n \sin n\phi + u_n' \cos n\phi) =$$

$$= -\psi_0 \sum \frac{n}{r_0} E_2 (v_n \sin n\phi + v_n' \cos n\phi). \quad \ldots(81)$$

The symbol $B_{r(r)}$ denotes the radial component of B_r. Let us adopt the following general expression for this quantity:

$$B_{r(r)} = B_r \sum w_n \sin n\phi + w_n' \cos n\phi. \quad \ldots(82)$$

Obviously, in a transversely-magnetised system, $w_1 = 1$, $w_{2\ldots n} = 0$, and $w_n' = 0$. But since we want to end up with a generally valid formula it will be better to take Eq.(82) as a basis for our further calculations, and to insert the numerical values of the coefficients at a later stage.

Eqs.(81) and (82) yield, on solving with respect to v_n and v_n',

$$v_n = \mu_{rev} \frac{r_0}{r_\alpha} \frac{E_1}{E_2} u_n - \frac{r_0 B_r}{\mu_0 n E_2 \psi_0} w_n, \quad \ldots(83)$$

$$v_n' = \mu_{rev} \frac{r_0}{r_a} \frac{E_1}{E_2} u_n' - \frac{r_0 B_r}{\mu_0 n E_2 \psi_0} w_n'. \quad \ldots(84)$$

These values inserted in Eq.(77) give

$$\psi_0 \sum \left[\left(D_1 - D_2 \mu_{rev} \frac{r_0}{r_a} \cdot \frac{E_1}{E_2} \right) u_n + D_2 \frac{r_0 B_r}{\mu_0 n E_2 \psi_0} w_n \right] \cdot \sin n\phi +$$

$$+ \left[\left(D_1 - D_2 \mu_{rev} \frac{r_0}{r_a} \cdot \frac{E_1}{E_2} \right) u_n' + D_2 \frac{r_0 B_r}{\mu_0 n E_2 \psi_0} w_n' \right] \cdot \cos n\phi = \psi_{0v}. \quad \ldots(85)$$

The following expression can be written for the potential ψ_{0v} of a pole-piece, in the interval $-\pi/2 < \phi' < \pi/2$:

$$\psi_{0v} = \psi_{0v} \sum \frac{4}{\pi} (-1)^{\frac{n+3}{2}} \frac{\cos n\phi'}{n} \quad \ldots(86)$$

The angle ϕ' is measured from the central axis of the pole-piece, and so $\phi = \phi_{01} + \phi'$. The function must be symmetrical with respect to this central axis.

From Eqs.(85) and (86) it is possible to derive a relationship between u_n and w_n, and another connecting u_n' and w_n'. The terms relating to even n values vanish; for odd n values,

$$\psi_0 \left(D_1 - D_2 \mu_{rev} \frac{r_0}{r_a} \frac{E_1}{E_2} \right) u_n =$$

$$= \psi_{0v} \frac{4}{\pi} (-1)^{\frac{n+3}{2}} \frac{\sin n\phi_{01}}{n} - D_2 \frac{r_0 B_r}{\mu_0 n E_2} w_n, \quad \ldots(87)$$

$$\psi_0 \left(D_1 - D_2 \mu_{rev} \frac{r_0}{r_a} \cdot \frac{E_1}{E_2} \right) u_n' =$$

$$= \psi_{0v} \frac{4}{\pi} (-1)^{\frac{n+3}{2}} \frac{\cos n\,\phi_{01}}{n} - D_2 \frac{r_0 B_r}{\mu_0 n E_2} w_n'. \quad \ldots(88)$$

It is now possible to eliminate u_n from Eqs.(83) and (87), and u_n' from Eqs.(84) and (88). In this way relationships between v_n and w_n, and between v_n' and w_n', can be arrived at; thereupon expressions involving w_n and w_n' can be substituted for v_n and v_n' in Eq.(72); and thus the following expression for the radial component of induction at $r = r_i$ can be derived from Eq.(79).

$$B_{L(r)}\big|_{r=r_i} =$$

$$= -\mu_0 \sum \frac{n}{r_0} E_2 \cdot \left\{ \left[\mu_{rev} \frac{r_0}{r_a} \frac{E_1}{E_2} \frac{\psi_{0v} \frac{4}{\pi} (-1)^{\frac{n+3}{2}} \frac{\sin n\phi_{01}}{n} - D_2 \frac{r_0 B_r}{\mu_0 n E_2} w_n}{D_1 - D_2 \mu_{rev} \frac{r_0}{r_a} \frac{E_1}{E_2}} - \frac{r_0 B_r}{\mu_0 n E_2} w_n \right] \sin n\phi + \right.$$

$$\left. + \left[\mu_{rev} \frac{r_0}{r_\alpha} \frac{E_1}{E_2} \frac{\psi_{0v} \frac{4}{\pi} (-1)^{\frac{n+3}{2}} \frac{\cos n\phi_{01}}{n} - D_2 \frac{r_0 B_r}{\mu_0 n E_2} w_n'}{D_1 - D_2 \mu_{rev} \frac{r_0}{r_a} \frac{E_1}{E_2}} - \frac{r_0 B_r}{\mu_0 n E_2} w_n' \right] \cos n\phi \right\}$$

$$= -\sum \left[\frac{\frac{\mu_0 \mu_{rev}}{r_a} E_1 E_2 \psi_{0v} \frac{4}{\pi} (-1)^{\frac{n+3}{2}} \cos n\phi'}{D_1 E_2 - D_2 \mu_{rev} \frac{r_0}{r_a} E_1} - \frac{B_r D_1 (w_n \sin n\phi + w_n' \cos n\phi)}{D_1 E_2 - D_2 \mu_{rev} \frac{r_0}{r_a} E_1} \right]. \quad \ldots(89)$$

For systems with a small magnet thickness ℓ and a small air-gap s, Eq.(89) can be further simplified. On taking $r_i = r_a - h$ and $r_i = r_0 + s$, the definitions of D_1 and D_2 given by Eq.(76) become

$$D_1 = -\frac{2nh}{r_a} \quad \ldots(90)$$

and,

$$D_2 = \frac{2ns}{r_0}. \quad \ldots(91)$$

Similarly, E_1 and E_2, as given by Eq.(80), can in first approximation be given a value of 2. Eq.(89) now reduces to,

$$B_{L(r)}\big|_{r=r_i} = \sum \left[\frac{\mu_0 \mu_{rev} \psi_{0v} \frac{4}{\pi} (-1)^{\frac{n+3}{2}} \frac{\cos n\phi'}{n}}{h + \mu_{rev} s} + \right.$$

$$\left. + \frac{h B_r (w_n \sin n\phi + w_n' \cos n\phi)}{h + \mu_{rev} s} \right]. \quad \ldots(92)$$

If we now make use of Eq.(86) and insert the numerical values $w_1 = 1$, $w_{2\ldots n} = 0$, and $w_n' = 0$, as appropriate to transverse magnetisation, we obtain:

$$B_{L(r)}\big|_{r=r_i} = \frac{h}{h + \mu_{rev} s} \left[\frac{\mu_0 \mu_{rev} \psi_{0v}}{h} + B_r \sin\phi \right]. \quad \ldots(93)$$

If, in addition, use is made of Eq.(24) it will be seen that the resulting expression corresponds to Eq.(25), provided that A and b_n in that equation are allotted certain values and all the harmonics are suppressed:

$$A = \frac{h}{h + \mu_{rev} s}{}^{*}, \quad b_n = 1 \text{ and } n = 1.$$

This means that we can apply the result of our calculations in the case of radial magnetisation (Eq.(41)) to transverse magnetisation. For example, within the limitations specified above the following expression is valid for the torque at position a:

$$M_a = 2 \frac{\ell \bar{r} s h \mu_{rev}}{(h + \mu_{rev} s)^2} N I B_r \sin\alpha \cos\phi_{01}. \quad \ldots(94)$$

Radial compared with Transverse Magnetisation

Eq.(94) reveals that a transversely-magnetised system is free from permanent magnetic pole sensitivity, the torque being the same as that obtained from a system that has been radially magnetised with the harmonic only (namely, a sinusoidal waveform). It will, however, be recalled that this is only true where h and s are sufficiently small compared to r_0, r_i and r_a, as is evident from the calculations just carried out.

For a given magnetic material, then, transverse magnetisation invariably yields a smaller torque value than radial magnetisation with the fundamental and the 3rd harmonic. This value can of course be raised by using material of higher remanence, – preferentially-oriented Magnadur for example. However, ring magnets with preferential orientation in a radial pattern are by no means easy to make: the contraction that accompanies sintering is much greater in the preferential direction than in the directions perpendicular to it, so that strong stresses are set up in the material. Motors embodying ring magnets or segments whose preferential orientation is transverse can be magnetised after assembly. However, the trouble is that if they are dismantled, the field may undergo irreversible weakening, because of the knee in the demagnetisation curves of these preferentially-oriented materials (Ref. 9). Magnets with preferential orientation in a radial pattern would of course be subject to the same disadvantage if treated likewise.

DESIGN HINTS

Armatures for the smaller class of d.c. motors with permanent-magnet field excitation are generally of the three-pole type, for economic reasons. In these small motors in particular, pole sensitivity is quite troublesome; but it can be avoided to a very great extent by magnetising with the fundamental plus 3rd harmonic, as referred to earlier. This magnetisation process yields a torque value about 15% greater than purely transverse magnetisation, which likewise produces no pole sensitivity.

The effect of pole sensitivity evens out when an armature with more than ten slots is employed. Motors with ratings from 10W to 100W are usually equipped with armatures of this kind, and the efficiency of the machines and the torque they deliver is generally a more important consideration than any slight unevenness in running. Radial square-wave magnetisation is therefore more advantageous in such systems, despite any pole sensitivity it may entail, for the resulting torque is 1·5 times greater than that obtained from a transversely-magnetised system.

The thickness of the ring magnet and the width of the air-gap will be fixed by economic and technological considerations. While a thick ring magnet invariably produces a greater flux density in the air-gap and so results in a higher torque, it has drawbacks in the shape of higher magnetic material costs and a tendency for the overall design to be cumbersome. On the other hand, considerations of mechanical strength will prevent reduction in the wall thickness of the ring. The efforts often made in the literature to arrive at an optimum set of dimensions for a magnet (Refs. 3, 4, 8), which require the placing of the working point at (BH_{max}), the point of highest energy density, do not represent the best policy in the design of the miniature motors we are concerned with here, for the resulting flux density is too small. Besides, where the use of preferentially-oriented magnet materials is contemplated, the resulting working point would be so low that any subsequent dismantling of the system would inevitably cause an irreversible weakening of the field magnet. One must, therefore, find a favourable compromise between the mutually conflicting requirements.

It is desirable that the air-gap should be as narrow as possible; but this implies close tolerances for the radial dimensions of the ring magnet, armature, and outer iron ring, and these in their turn will mean high production costs. In this respect, too, the designer must look for a compromise.

---

*This expression for A is obtained in place of Eq.(15) when H_M and H_L in the line integrals

$$\int_{r_i}^{r_a} H_M d_r \text{ and } \int_{r_0}^{r_i} H_L d_r$$

are regarded as constant; that is, as equal to $H_M h$ and $H_L s$ respectively, as is quite permissible for narrow air-gaps adjoining thin ring magnets. The magnetic potential ψ_{0v} appearing in Eq.(3) corresponds to the expression $2NI/3 + \text{const.}$, in Eq.(20).

Design of small D.C. Motors embodying Magnadur Permanent Magnets

M. F. Reynst
Philips' Icoma Laboratories, Eindhoven

This article presents a method of dimensioning d.c. motors with normal multi-slot armatures. In contrast to the usual practice, the more important electrical quantities like efficiency, operating current, and back e.m.f. are laid down from the outset in this method; principal dimensions like rotor length and diameter are not arrived at until the end of the design calculations. This dimensioning method has been worked out with particular reference to d.c. motors equipped with Magnadur magnets and having powers between 10 and 100W. Fractional h.p. motors of this kind are now employed on a large scale, mainly as auxiliary equipment in road vehicles; they are also being used more and more for household appliances which are battery-operated, and hence independent of mains supplies.

One of the advantages of the dimensioning method presented is that the desired electrical efficiency is treated like any other electrical design quantity, instead of merely resulting from the other data after the geometrical and electrical dimensions have been calculated; a practice which may necessitate complete re-dimensioning of the motor. The relationship between operating torque and starting torque is also very straightforward in this method. The calculations which follow are based on medium-size motors embodying segmental field-magnets made of preferentially-oriented Magnadur whose remanence lies between about 3500 × 10⁻⁸ and 4000 × 10⁻⁸ Vs/cm². Where the armature is of the multi-slot type, 'pole sensitivity' is negligible.

INTRODUCTION

Permanent magnets for small d.c. motors can either be made from a steel alloy or the ceramic material Magnadur. The choice between the two types of material is determined, among other things, by the geometrical dimensions and the allowed cost of the motor.

Since the magnetic field remains more or less constant while under load, motors of this kind behave, in principle, like shunt-wound machines. Generally speaking, where the field magnet is of Magnadur the flux density in the air-gap attains a value between 2000×10^{-8} and 4000×10^{-8} Vs/cm². Being relatively insensitive to demagnetising fields, Magnadur magnets can be made flat; that is to say, it is possible for the wall thickness of ring magnets or segments to be small in comparison with their radius. However, it is necessary, from the production point of view, that the magnets should have simple geometrical shapes.

Where steel magnets are employed, the cheapest design in a given case is generally that which minimises the bulk of the magnetic material. With Magnadur magnets, on the other hand, the optimum magnetic configuration from both the operational and technological points of view is not usually the best design, because it results in a ring magnet with an undue thinness of wall. A rather thicker ring magnet is more convenient to manufacture, although its working point is higher than necessary. Whenever d.c. motors with permanent-field magnets are designed it is wise to consider, from the outset, the properties of the permanent magnet material.

If a certain flux value is worked out from electrical and mechanical data, there will be no guarantee that this particular flux can actually be obtained from Magnadur in an economical manner. The position is different when electromagnets are to be used: then practically any normal value of flux can be obtained merely by increasing the number of turns, or stepping up the energising current, or both. Nevertheless, permanent magnets can have distinct advantages in field excitation in a fractional h.p. motor.

DESIGN FUNDAMENTALS

Data Required

We shall assume that the no-load voltage V_L and internal resistance R_i of the voltage source are both known. Fractional h.p. motors are generally supplied from an accumulator, a dry battery, or a rectifying set. The usual source in road vehicles is a 6V or a 12V accumulator. Provided IR_i is negligible compared with V_L, it is alternatively possible to use V_k, the terminal voltage (source), in the calculations.

Generally the designer is given the required torque M_n at a stated motor speed n. This must definitely be specified when the motor is to be directly coupled to a device being driven, such as a fan. Sometimes, however, when there is to be gearing between the motor and this device, only the product $M_n n$ is of interest to the designer, this representing the mechanical power P_n delivered by the motor. The relationship between the two is given by the well-known formula:

$$P_n = M_n n.\ 1{\cdot}03.\ 10^{-5}. \qquad \ldots(1)$$

where P_n is in W, M_n is in pcm, n is in rev/min.
Torque M_n is proportional to the volume of the armature. For example, when it is desired, for price reasons, that a motor of a given wattage should have the smallest possible geometrical dimensions, the endeavour will be to increase the speed. Obviously, the speed of the motor being subject to limitations imposed by: wear on the brushes, the voltage drop across the contact resistance between brush and commutator bars, commutation problems, and the efficiency of the motor and gearing, cannot be increased indefinitely. In addition, requirements are likely to be imposed on the starting torque, current drain, and electrical efficiency. Clearly, it will often be necessary to find a compromise when a number of such requirements have to be met.

Torque Equation

It is usual to define various kinds of motor efficiency. If P_m denotes the total mechanical output of the motor, V_k the voltage across its terminals, and I the current through the armature, then its electrical efficiency, determined by the voltage drop across the armature windings and brushes (the ohmic losses I^2R_t) will be,

$$\eta_e = \frac{P_m}{V_k I}. \qquad \ldots(2)$$

Small machines have widely differing electrical efficiencies η_e ranging between 20% and 90%. The value tends to depend on the purpose and size of the motor. If P_n is the useful output from the motor at n r.p.m., its mechanical efficiency, governed by frictional losses and to some slight extent by iron losses too, will be:

$$\eta_m = \frac{P_n}{P_m} = \frac{P_m - P_v}{P_m}. \qquad \ldots(3)$$

Here the sum of the above losses is denoted by P_v. The product of η_e and η_m is known as the overall efficiency η_{tot}.

$$\eta_{tot} = \eta_e \eta_m = \frac{P_n}{V_k I}. \qquad \ldots(4)$$

The e.m.f. V_o induced by armature movement is the difference between the terminal voltage V_k, and the voltage loss V_v at the armature and brushes:

$$V_o = V_k - V_v. \qquad \ldots(5)$$

The rate at which work is done on turning the armature is given by:

$$P_m = V_k I - V_v I, \qquad \ldots(6)$$

where $V_k I$ is the total power taken up by the motor and $V_v I$ is the wattage consumed in the armature and brushes. Accordingly, we can write down the following for the electrical efficiency:

$$\eta_e = \frac{V_k I - V_v I}{V_k I} = \frac{V_o}{V_k}. \qquad \ldots(7)$$

The voltage induced across the armature is alternatively given by,

$$V_o = \frac{p}{a} z \Phi \frac{n}{60} \cdot 10^{-8}, \qquad \ldots(8)$$

where V_o is in V, Φ is in maxwell, n is in rev/min.
In this expression, p is the number of pole-pairs, 2a the number of current paths through the armature (which is the same as the number of brushes), z the number of armature turns, and Φ the flux entering the armature from one pole-piece. This last is dependent on the current through the motor:

$$\Phi = \Phi_o - aI \qquad \ldots(9)$$

where Φ_o is the flux at I = 0 and a, roughly speaking, represents a constant. For d.c. motors rated up to 100W and equipped with Magnadur magnets it is usually permissible to make $\Phi = \Phi_o$ in a first approximation.

Eqs.(1), (3), (6), (5), and (8) yield the following expression for the torque M_n:

$$M_n = \eta_m \frac{p}{a} z \Phi I_n . 1{\cdot}62 . 10^{-5}. \qquad \ldots(10)$$

where M_n is in pcm, Φ is in maxwell, I_n is in A.
In this expression, I_n is the armature current at a motor speed of n revolutions per minute.

Since the terminal voltage is

$$V_k = V_L - I_n R_i, \qquad \ldots(11)$$

we can write, using Eq.(5):

$$V_L - I_n R_i = V_o + V_v = V_o + I_n R_t, \qquad \ldots(12)$$

where R_t is the sum of the armature resistance R_a, the brush resistance R_b, and any ballast R_v that may be inserted. With the aid of Eqs.(8), (10) and (12), and eliminating I_n, we obtain:

$$M_n = \eta_m \frac{pz\Phi \cdot 1 \cdot 62 . 10^{-5}}{a(R_i + R_t)} \left[V_L - \frac{p}{a} z \Phi \frac{n}{60} \cdot 10^{-8} \right]. \qquad \ldots(13)$$

where M_n is in pcm, Φ is in maxwell, R_i is in Ω, R_t is in Ω, V_L is in V, n is in rev/min.

If now we put $p\,\Phi = \Phi_t$ and $a = 1$ (that is, if we assume that the armature offers two current-paths, the motor having been fitted with two brushes, which is usually the case in small motors), we arrive at the following value for the total torque created by the motor, inclusive of losses:

$$M_m = \frac{P_m}{n} \cdot 0{\cdot}97 \cdot 10^5 = \frac{M_n}{\eta_m} = \frac{1{\cdot}62 . 10^{-5} z \Phi_t}{R_i + R_t} [V_L - z\Phi_t n . 1{\cdot}66 . 10^{-10}]. \qquad \ldots(14)$$

where M_m is in pcm, P_m is in W, n is in rev/min, M_n is in pcm, Φ_t is in maxwell, R_i is in Ω, R_t is in Ω, V_L is in V.

Maximum Torque

The value of the product $z\Phi_t$ for which the torque is maximum, proves to be:

$$z\Phi_t = \frac{V_L}{n} 3 . 10^9. \qquad \ldots(15)$$

where Φ_t is in maxwell, V_L is in V, n is in rev/min.

The maximum torque itself is obtained by inserting the above in Eq.(14).

$$M_{m\,max} = \frac{M_{n\,max}}{\eta_m} = \frac{V_L^2}{n(R_i + R_t)} \cdot 2{\cdot}43 . 10^4. \qquad \ldots(16)$$

where $M_{m\,max}$ is in pcm, $M_{n\,max}$ in pcm, V_L in V, R_i in Ω, R_t in Ω, n in rev/min. Also, Eqs.(8) and (15) yield,

$$V_o = V_L/2. \qquad \ldots(17)$$

Insertion of the above in Eq.(12) reveals that the back e.m.f., generated by the motor, is equal to the total of voltage drops within the circuit when the torque has its maximum value. Also, $I_n$max, the current flowing when the maximum torque is being delivered, can now be readily worked out from Eq.(12).

$$I_{n\ max} = \frac{1}{2}\frac{V_L}{R_i+R_t}. \qquad \ldots(18)$$

The starting current has twice this magnitude; thus

$$I_0 = V_L/(R_i+R_t) \qquad \ldots(19)$$

The starting torque under these conditions can be derived from Eqs.(10) and (19) on putting $\eta_m = 1$ (the assumption being that there are no frictional or iron losses).

$$M_{m0\ max} = M_{n0\ max} = \frac{{V_L}^2}{n(R_i+R_t)} \cdot 4 \cdot 86.10^4 \qquad \ldots(20)$$

where $M_{m0\ max}$ is in pcm, $M_{n0\ max}$ is in pcm, V_L is in V, R_i is in Ω, R_t is in Ω, n is in rev/min.

Thus the starting torque is twice that at the rated turning-speed.

If in the efficiency equation (see Eq.(7)),

$$\eta_e = \frac{V_o}{V_k} = \frac{V_o}{V_L - I_n R_i}, \qquad \ldots(21)$$

then it is permissible to neglect the product $I_n R_i$, since it is small compared with V_L. So it follows that:

$$\eta_e = V_o/V_L. \qquad \ldots(22)$$

Insertion of Eq.(17) in the above yields an electrical efficiency value of 50%. Estimating the mechanical efficiency at about 80%, we find that the overall efficiency* of the motor (Eq.(4)) is about $\eta_{tot} = 40\%$.

Briefly, the following can be said about equations (14) to (20). Eq.(14) represents the general formula for the torque M_m, it being assumed that V_L, R_i, and n are as given, and that R_t and product $z\Phi_t$ are determined by the general design of the motor. Alternatively, $z\Phi_t$ can be obtained from Eq.(15), which yields the value appropriate to a maximum M_m. However, if M_m is one of the given parameters it also determines R_t, from Eq.(14); in this case $I_{n\ max}$, I_o, $M_{m0\ max}$, and η_e, all follow from Eqs.(16) to (21).

The $M_m = f(z\Phi_t)$ Curves

In order to investigate other design possibilities, for example where a different efficiency figure is required, the simplest procedure is to make use of the graphs described in the next section.

Fig. 1 is a plot of torque as a function of $z\Phi_t$ based on Eq.(14), in which $R_t = R_a + R_b$ is the variable parameter. The values of the parameters held constant are given in the caption to the graph. It will be seen that in this particular case M_m reaches a peak at $z\Phi_t = 18 \times 10^6$, and that it is zero at $z\Phi_t = 0$. The reason is that if no load is placed on the motor, and no losses occur (on the assumption of an ideal machine), then $I_n = 0$ and $V_L = V_o$. In this case, too, the motor has a speed of n = 2000 rev/min.

If a still larger value were chosen for $z\Phi_t$, then M_m would become negative; in fact, mechanical power would have to be supplied from outside, and at 2000 rev/min. the machine would generate a voltage V_o, greater than V_L. In other words, the motor would be functioning as a generator.

The situation at the maxima of the curves is expressed by Eqs.(15) to (20). For all points on these curves, the electrical efficiency can be obtained from Eq.(21). Where it is possible to use Eq.(22), the simplified version, one can take account of Eq.(8) and so obtain the following expression for electrical efficiency:

$$\eta_e = \frac{V_o}{V_L} = \frac{z\Phi_t}{36.10^6} \qquad \ldots(23)$$

where Φ_t is in maxwell.

In such a case, the scale of η_e can simply be marked off along the abscissa.

Other things being equal, a higher efficiency can only be obtained by increasing the flux or the number of armature turns, or both. Generally, the result of doing so is to increase the size of the motor. If, on the other hand, a lower efficiency suffices, the required $z\Phi_t$ will be smaller, as will the size of the motor. Where a certain degree of efficiency is required at a certain torque, the required $z\Phi_t$ and resistance R_t can be obtained by referring to Fig. 1. The curve of $R_t = f(z\Phi_t)$ in Fig. 2, which likewise derives from Eq.(14), may also be useful here.

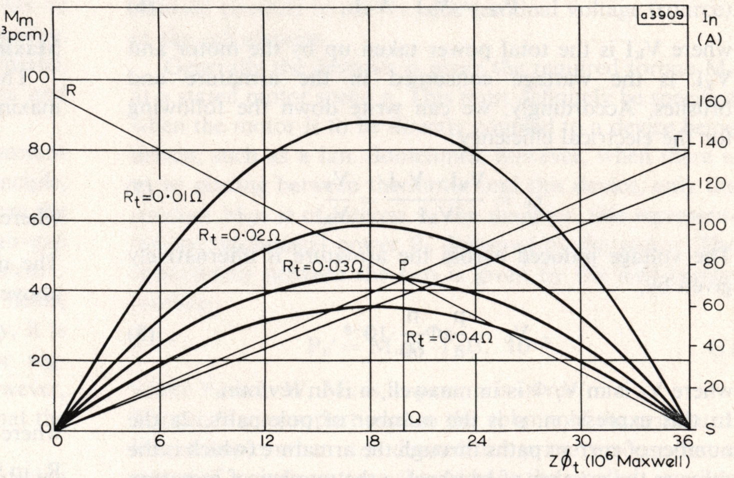

Fig. 1—Torque versus $z\phi_t$ for various values of R_t, with V_L = 12V, n = 2000rev/min, R_i = 0·01Ω

---

*Small motors are required to run at the highest possible speed. With larger motors the situation is different: these are required to have a higher efficiency, otherwise losses are excessive and overheating will occur. The following list of overall efficiencies for differing motor wattages will serve as a rough guide.

up to 1W	20% to 40%
from 1W to 3W	up to 50%
from 3W to 10W	up to 60%
10W and over	up to 70%

In small motors with ratings up to 1W, the losses are due almost exclusively to brush friction.

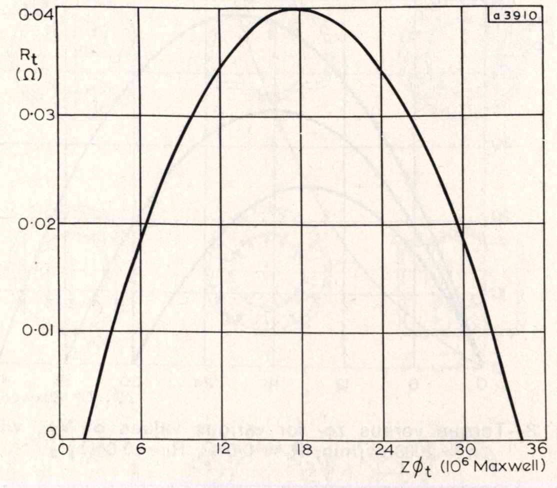

Fig. 2—R_t versus $z\phi_t$, with V_L = 12V, n = 2000rev/min, M_m = 35kpcm, R_i = 0·01Ω

Thus, the maxima of the various parabolas in Fig. 1 represent the maximum torque delivered by different motors with the same $z\Phi_t$ product. Table 1 gives an idea of the corresponding power outputs. The values relate to motors with a mechanical efficiency of 80%, and do not take account of armature reaction. Other parameters have the values given in the caption to Fig. 1.

Determination of Starting Torque and Motor Current

From Fig. 1 the starting torque corresponding to steady running at any point of the $M_m = f(z\Phi_t)$ parabolas can be determined. If a straight line is drawn from point S (the point at which the parabolas intersect with the abscissa on the right) through a point (say P) on one of the parabolas, its point of interception on the left-hand ordinate (R) will represent the corresponding starting torque. The correctness of this construction can be proved in the following way.

The torque M_m at any point P on one of the parabolas, represented by PQ in Fig. 1, is given by

$$M_m = a[b\,z\Phi_t - c(z\Phi_t)^2], \qquad \ldots(24a)$$

where, a, b, and c are constants (see Eq.(14)). The starting torque can likewise be obtained from Eq.(14) by putting n = 0:

$$M_{m0} = a\,b\,z\Phi_t. \qquad \ldots(24b)$$

Accordingly, the ratio between the two torques is:

$$\frac{M_m}{M_{m0}} = 1 - \frac{c}{b} z\Phi_t. \qquad \ldots(25)$$

But we also have, at intercept S,

$$M_m = a[b\,z\Phi_t - c(z\Phi_t)^2] = 0 \qquad \ldots(26a)$$

and hence:

$$(z\Phi_t)_{max} = b/c \qquad \ldots(26b)$$

allowing us to write the following equation

$$\frac{\overline{PQ}}{\overline{RO}} = \frac{\overline{SQ}}{\overline{SO}} = \frac{\frac{b}{c} - z\Phi_t}{\frac{b}{c}} = 1 - \frac{c}{b} z\Phi_t. \qquad \ldots(27)$$

The expression on the right is in fact the same as in Eq.(25), showing the correctness of the construction given above.

TABLE 1

Calculated values of total and useful power delivered at maximum torque by a series of motors having different R_t values, and the same $z\Phi_t$ (18×10⁶ maxwell). n = 2000 rev/min and η_m = 80%.

R_t(Ω)	P_m(W)	P_n(W)
0·01	1800	1400
0·02	1200	936
0·03	900	725
0·04	721	576

Finally, the current I_n flowing at the rated motor speed n can be conveniently derived from Fig. 1. To do this, a perpendicular is erected at S, and a straight line is drawn from the origin O through the point P, to cut this perpendicular at point T. The length of line ST on the right-hand ordinate indicates the value of I_n, as the following shows.

Solving Eq.(10) with respect to I_n we obtain

$$I_n = \frac{M_m}{z\Phi_t} \cdot \frac{10^5}{1 \cdot 62}. \qquad \ldots(28)$$

where M_m is in pcm, Φ_t is in maxwell.

Now M_m is proportional to $\overline{PQ}$, and $z\Phi_t$ is proportional to $\overline{OQ}$, hence

$$I_n = C\frac{\overline{PQ}}{\overline{OQ}} = C\frac{\overline{ST}}{\overline{OS}} = C'.ST, \qquad \ldots(29)$$

where C and C′ are constants. That is to say, ST is proportional to current I_n. The scale for the right-hand ordinate is found by drawing a straight line through the origin and through the maximum of any of the parabolas. Its point of interception on the perpendicular erected at S gives the value determined by Eq.(18), namely $V_L/(2(R_i+R_t))$. This relates a point on the right-hand ordinate to a definite value on the I_n scale. Thus, the value of I_n = 120mA is determined from the parabola relating to R_t = 0·04Ω.

Curves relating to different Motor Voltages and different Motor Speeds

The treatment of design fundamentals will be concluded by describing two further sets of $M_m = f(z\Phi_t)$ curves which can be of value in the design of d.c. motors.

In Fig. 3, voltage V_L is the variable parameter, all other parameters being held constant. Here the maximum torques occur at different $z\Phi_t$ values, all lying on the parabola

$$M_{m\ max} = 1 \cdot 08.10^{-10}(z\Phi_t)^2 = 2 \cdot 43.10^2 {V_L}^2, \qquad \ldots(30)$$

where $M_{m\ max}$ is in pcm, Φ_t is in maxwell, V_L is in V. The coefficients in the above equation have been evaluated from Eqs.(15) and (16). The equation shows that as the motor voltage increases, the torque remaining the same, efficiency can be improved by increasing $z\Phi_t$. If, on the other hand, this latter product is kept constant, raising the motor voltage will produce a fall-off in efficiency.

The motor speed n is the variable parameter in Fig. 4. Maximum torques can occur at differing $z\Phi_t$ values, but here they lie along a straight line given by:

$$M_{m\ max} = 1{\cdot}945.10^{-3} z\Phi_t = \frac{7{\cdot}0.10^7}{n}. \qquad \ldots(31)$$

where $M_{m\ max}$ is in pcm, Φ_t is in maxwell, n is in rev/min.

DESIGN PROCEDURE

Before a practical example of design can be embarked upon, the quantities Φ, z, η_m, and R_t must be determined either by calculation or measurement. The weight of copper yielded by these calculations must, somehow, be accommodated in an armature having dimensions d_0 and ℓ_A; the required amount of flux must be created and constrained in order to pass through the armature. Here an important part may be played by the dimensions and permissible heat dissipation.

It must be stressed that the routine described below is not complete. In a more exhaustive analysis, other influences such as armature reaction and saturation effects must be considered.

Magnetic Flux Values in the Unloaded Motor

Some of the possible magnet arrays

Diagrams (a) to (o) in Fig. 5 show some of the ways of arranging the permanent field magnets in d.c. motors. Their main purpose is to allow the reader to compare the various design possibilities for motors with permanent-magnet field excitation. The choice between these is to some extent governed by cost. Only the designs shown in Fig. 5(a), (b), and (c) will be dealt with.

Two-pole d.c. motors can be profitably equipped with two segments made of preferentially-oriented Magnadur that has a sufficiently high coercive force (Magnadur 3 improved version, for example). In the magnet arrays to be described here, the direction of orientation and magnetisation is diametric. Materials with preferential orientation in the radial direction are most advantageous where the subtended angle β is large (Fig. 6), but it is not always feasible to produce such segments from anisotropic Magnadur to the desired dimensions. The magnetic circuit is completed by an iron ring whose thickness should, if possible, be large enough to bring the flux density inside it to within the limit of 14000×10^{-8} Vs/cm².

The Magnadur segments can be fixed inside the iron ring with a suitable adhesive; alternatively, the space between the segments can be filled with, for example, polyester resin. The third possibility is to hold the segments in position with compression springs inserted between the flattened end-faces marked A in Fig. 7.

Fig. 7 shows a Magnadur segment with exact dimensional and tolerance data. Fig. 8 will serve to show how these tolerances work out in practice. In the latter diagram, the segment just conforming to the outside tolerance limits is fully drawn, and its convex face lies flush against the inside of the iron ring, while its concave face is clear from the armature by 0·5mm all round (0·5mm being the normal gap width). The segment just conforming to the lower tolerance limits has only the two edges of its convex face in contact with the iron ring, leaving a narrow air-gap in between. The air-gap on the concave side is larger here, especially at its right-hand and left-hand extremities. The width of the segment is also smaller. All these deviations from the normal shape result in a loss of flux; the difference between the maximum and minimum flux values may amount to as much as 20%.

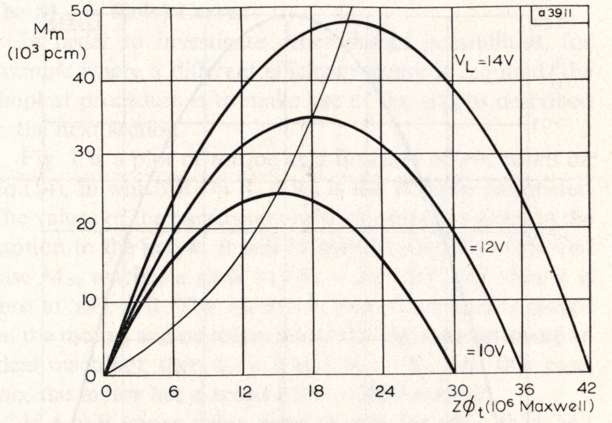

Fig. 3—Torque versus $z\phi_t$ for various values of V_L, with n = 2000rev/min, $R_i = 0{\cdot}01\Omega$, $R_t = 0{\cdot}04\Omega$

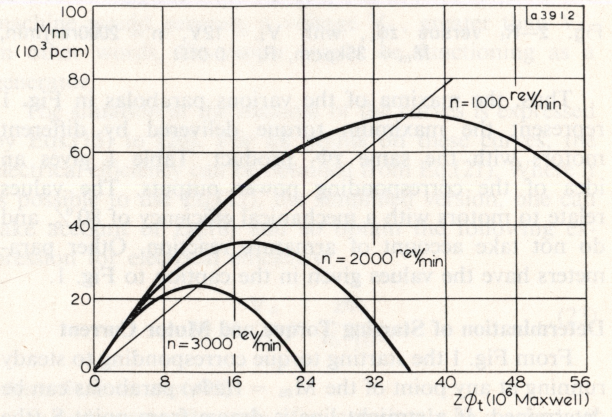

Fig. 4—Torque versus $z\phi_t$ for various speeds, with $V_L = 12V$, $R_i = 0{\cdot}01\Omega$, $R_t = 0{\cdot}04\Omega$

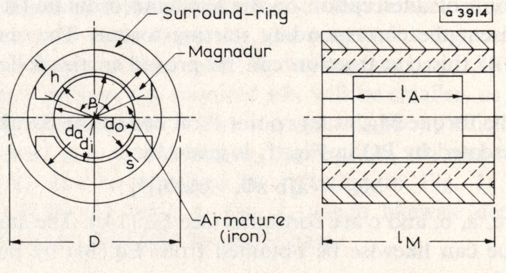

Fig. 6—Key to symbols used for motor dimensions

The angle β subtended by the segments should not be too great, otherwise the best use cannot be made of the transverse magnetisation of the material; preferably, β should be less than 120° and should in no case exceed 140°. In the case of radial magnetisation, β should preferably be less than 140°.

In the designs shown in diagrams (a) and (f), one segment can be replaced by a block of iron of the same shape, or can be eliminated by conferring a suitable shape on the iron frame, which serves as the frame magnet (see diagram (b)). If this is done, the resulting lack of magnetic balance, and the leakage that inevitably accompanies it, will lead to a roughly 10% greater flux in the air-gap adjacent to the Magnadur segment than that in the gap on the opposite side. This figure of 10% has been measured on an actual example, but the flux can also be worked out by the method given on page 218, using 2s instead of 1s. In further calculations, one must work with a smaller, average flux value. However, it is sometimes possible to increase the flux in the air-gap adjacent to the iron segment, by making the latter somewhat wider, so that it subtends a larger value of β. Whether this can be done or not depends on the number of slots in the armature; moreover, where the segments carrying the armature windings are smaller than the Magnadur or iron segment, the flux that is effective in creating torque depends to some extent on the pitch of the windings.

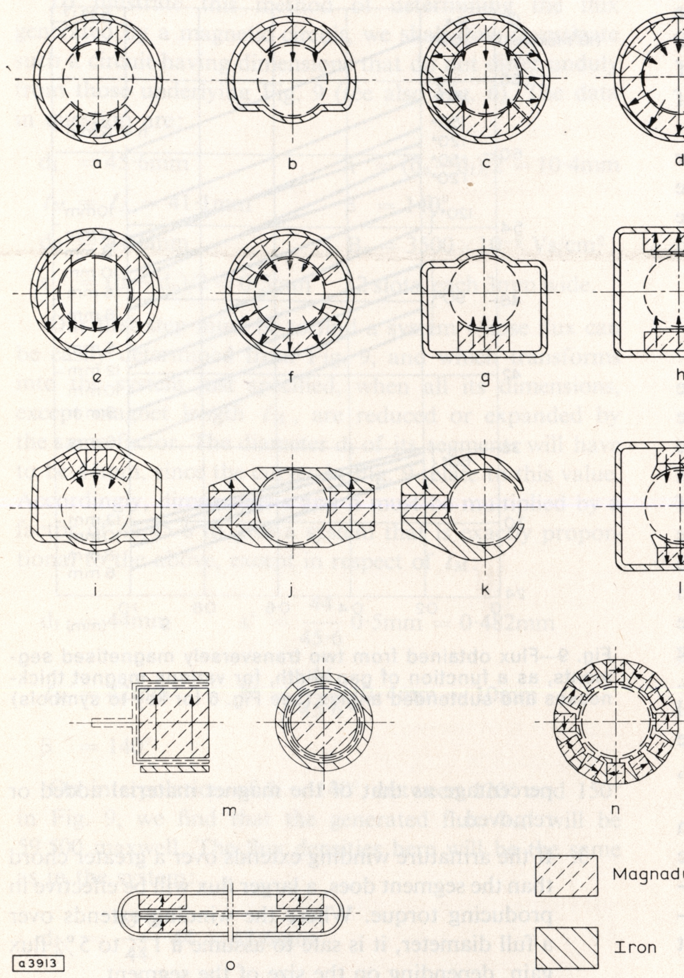

Fig. 5—Configurations of d.c. motors with permanent magnet field excitation. The arrows indicate the direction of magnetisation

(a) to (c): see text
(d), (e): discussed in Ref. 15
(j) to (l): unsatisfactory flux distribution, (k) in particular exhibiting excessive leakage
(m), (o): have ironless armatures
(n): may be suitable for large motors with strong fields, but cost is rather high

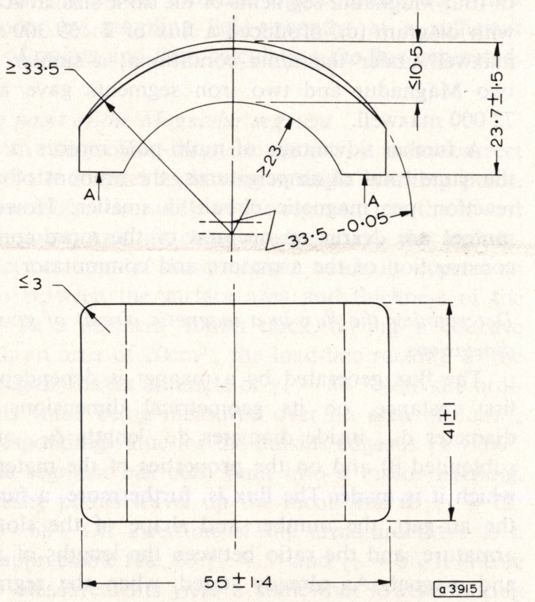

Fig. 7—Magnadur segment for small d.c. motor, with dimensions in mm

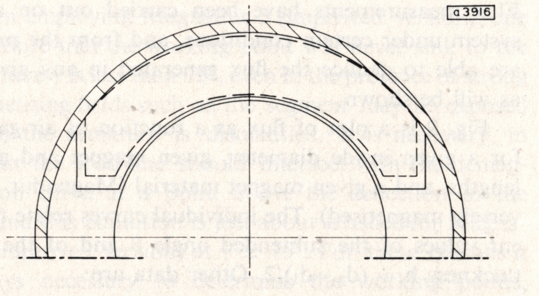

Fig. 8—Segment in position, showing effect of tolerances

Again, since the Magnadur segment is loaded with the reluctance of the two air-gaps facing it, its working point is lower than when two Magnadur segments are used. For this reason, the Magnadur segment built into the non-balanced design should have rather greater depth; even then, the motor may still be cheaper than one equipped with two such segments.

An appreciably greater Φ_t for the same diameter can be obtained by building the motor with more than two pole-pieces, as in diagram (c). The usual practice is to surround the rotor entirely with magnetic material. The flux thus created can be determined in approximation by the method described on page 218. It has been found, however, that the flux actually present in this design is about 7% lower than the calculated value. Half of the Magnadur segments in this design can be replaced by iron ones.

Here, by way of example, are some comparative data on three different arrays. With an array of two Magnadur segments each subtending an angle of 90°, a flux value of Φ_t = 41 300 maxwell is obtained. A four-pole array of four Magnadur segments of the same size, in accordance with diagram (c), produced a flux of $2 \times 39\,300 = 78\,600$ maxwell under the same conditions; a similar array of two Magnadur and two iron segments gave a flux of 72 000 maxwell.

A further advantage of multi-pole motors is that, for the same total of ampere-turns, the amount of armature reaction per magnetic circuit is smaller. However, the motors are dearer on account of the more complicated construction of the armature and commutator.

Determining the flux in a magnetic circuit of given dimensions

The flux generated by a magnet is dependent, in the first instance, on its geometrical dimensions (outside diameter d_a, inside diameter d_i, length ℓ_M, and angle subtended β) and on the properties of the material from which it is made. The flux is, furthermore, a function of the air-gap, the number and shape of the slots in the armature, and the ratio between the lengths of armature and magnet. As already stated, when the segments on which the armature coils are wound are smaller than those of the magnet system, the flux actually effective in creating torque is dependent also on the pitch of the windings. Flux measurements have been carried out on a model system under certain conditions, and from the results we are able to deduce the flux generated in any given case, as will be shown.

Fig. 9 is a plot of flux as a function of air-gap width for a given inside diameter, given magnet and armature lengths, and a given magnet material (Magnadur 3, transversely magnetised). The individual curves relate to different values of the subtended angle β and of the magnet thickness $h = (d_a - d_i)/2$. Other data are:

$d_i = 44\text{mm}$

$\ell_M = \ell_A = 42\text{mm}$

$B_r = 3550 \times 10^{-8}\ \text{Vs/cm}^2$.

The flux was measured along a chord of the segment, from one outside edge to the other; the iron armature core was unslotted. Now, flux densities remain unchanged when a magnetic circuit is scaled up or down, the flux itself increasing or decreasing as the square of the dimensional increases or decreases. By virtue of this fact, Fig. 9 can be used to determine the flux generated in magnetic circuits having a set of geometrical dimensions different from, but proportional to, those noted above. Other kinds of deviation can be allowed for in accordance with the following:

1. Where the number of slots is between 6 and 15, an approximately 3% loss of flux can be assumed. For the same surface area of iron in the armature relative to that of the segment, a small number of wide slots is associated with a lower flux than a large number of narrow ones.
2. The angle β subtended by the segment is measured from the inner arc; the curves appearing in Fig. 9 relate to segments whose inner and outer arcs subtend the same angle. Where there is a difference between the angles subtended by the inner and outer arcs, the flux increases or decreases by the same percentage as that of the magnet material added or removed.

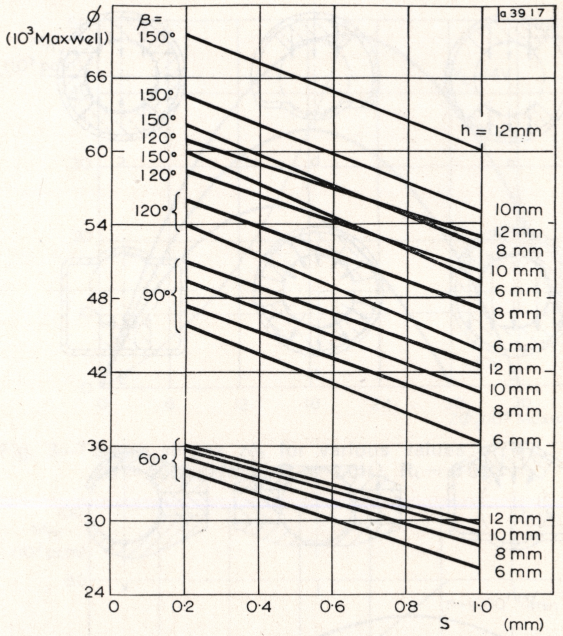

Fig. 9—Flux obtained from two transversely magnetised segments, as a function of gap width, for various magnet thicknesses and subtended angles (see Fig. 6 for key to symbols)

3. If the armature winding extends over a greater chord than the segment does, a larger flux will be effective in producing torque. Where the winding extends over a full diameter, it is safe to assume a 1% to 5% flux gain, depending on the size of the segment.
4. The curves in Fig. 9 are appropriate to material having a remanence of $3550 \times 10^{-8}\ \text{Vs/cm}^2$. Where the material employed has a remanence B_r differing from this, the flux value determined from the diagram must be multiplied by the factor $B_r/3550 \times 10^{-8}\ \text{Vs/cm}^2$.
5. It is always advantageous to make the magnet rather longer than the armature. In this way a higher flux is obtained without an appreciable increase either in the size of the motor or in its cost. Fig. 10 shows the percentage gain as a function of ℓ_M/ℓ_A, the ratio between the magnet and armature lengths.

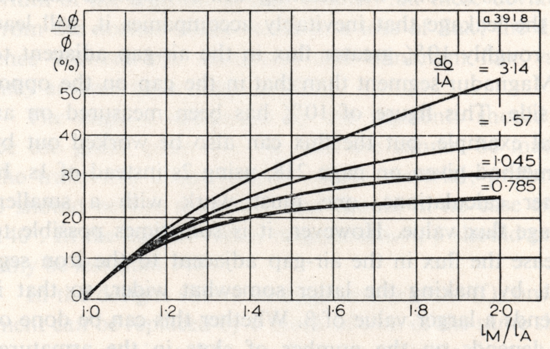

Fig. 10—Increase of flux obtained by increasing the ℓ_M/ℓ_A ratio

To illustrate this method of determining the flux generated by a magnetic circuit, we shall now investigate such a circuit having dimensions that do not differ unduly from those underlying Fig. 9 (see also Fig. 6). The data in question are:

$d_i = 45{\cdot}6\text{mm}$ $\qquad h = (d_a - d_i)/2 = 10{\cdot}4\text{mm}$

$\ell_M = \ell_A = 41{\cdot}1\text{mm}$ $\qquad \beta = 140°$

$d_o = 44{\cdot}6\text{mm}$ $\qquad B_r = 3500 \times 10^{-8}\ \text{Vs/cm}^2$

$s = (d_i - d_o)/2 = 0{\cdot}5\text{mm}$ $\qquad$ 12 slots, each 3mm wide.

Our first step must be to find a system whose flux can be easily determined from Fig. 9, and which transforms into the system just specified, when all its dimensions, except magnet length ℓ_M, are reduced or expanded by the same factor. The diameter d_i of its segments will have to be 44mm, since the curves in Fig. 9 relate to this value. Accordingly, dimensions s and h must be multiplied by a factor of 44/45·6 to give a system that is exactly proportional to the above, except in respect of ℓ_M:

$$d_i = 44\text{mm} \qquad s' = \frac{44}{45{\cdot}6}\,0{\cdot}5\text{mm} = 0{\cdot}482\text{mm}$$

$$\ell_M' = 42\text{mm} \qquad h' = \frac{44}{45{\cdot}6}\,10{\cdot}4\text{mm} = 10\text{mm}$$

$$\beta = 140°$$

On interpolation of $\beta = 140°$, between 120° and 150° in Fig. 9, we find that the generated flux Φ_m' will be 59 500 maxwell. The flux densities here will be the same as in the system:

$$d_i = \frac{45{\cdot}6}{44} \cdot 44 = 45{\cdot}6\text{mm}$$

$$\ell_M'' = \frac{45{\cdot}6}{44} \cdot 42 = 43{\cdot}5\text{mm}$$

$$s = \frac{45{\cdot}6}{44} \cdot 0{\cdot}482 = 0{\cdot}5\text{mm}$$

$$h = \frac{45{\cdot}6}{44} \cdot 10 = 10{\cdot}4\text{mm}$$

However, the total amount of flux created by this latest modification will be greater by a factor of $(45{\cdot}6/44)^2 = 1{\cdot}08$. We have still to allow for the fact that $\ell_M = 41{\cdot}1\text{mm}$ in the required system. We can do so by further multiplying the flux by the factor of $41{\cdot}1/43{\cdot}5 = 0{\cdot}945$. Again, the difference in remanence means that yet another factor, amounting to $3500/3550 = 0{\cdot}985$, must be applied. Lastly, the slots are responsible for a flux fall-off of about 3%, corresponding to multiplication by a factor of 0·97. Applying these correction factors, then, we arrive at the following value for the flux in the required design:

$$\Phi_m = 59\,500\,.\,1{\cdot}08\,.\,0{\cdot}945\,.\,0{\cdot}985\,.\,0{\cdot}97 = 58\,000\ \text{maxwell}.$$

There are various other ways of determining flux. The simplest is to run the machine as a dynamo and to evaluate Φ from Eq.(8). Thus, the flux present under no-load is arrived at. Approximately the same result will be obtained if the flux is measured physically with a probe and ballistic galvanometer; the armature can be turned through a given angle, so as to produce a change in the flux passing through the probe coil. Flux can also be measured with a Hall probe, by sampling field-strengths at a sufficient number of points and then calculating the flux generated.

Working point of the Magnadur segment

As with many other magnetic circuits, it is not correct to regard the magnet as having a single working point. Before assembly, the middle of the segment has the lowest working point, and its outside edges have the highest. The exact positions of these maxima naturally depend on the ratio between the surface area and thickness of the segment. In a segment 10mm thick, having a concave face with an area of 20cm², the load-line relating to the middle region makes an angle of $\gamma_1 = 88°$* with the ordinate, this value being measured over an area of 1cm²; the corresponding value for the outside edges is $\gamma_2 = 80°$. Once the segment has been built into a motor housing, the working points travel up the recoil line to $\gamma_1 = 72°$ and $\gamma_2 = 68°$. On insertion of the armature there is a further appreciable rise, to $\gamma_1 = 3°$ and $\gamma_2 = 5°$. It is true that the measurements yield a somewhat lower working point for the edges of the segment, the reason being that flux-leakage here interferes with the accuracy of the measurements.

When employing Magnadur 3 (improved version), one must ensure that the working point will never sink to the point where γ is less than 75°, even in the presence of strong demagnetising fields such as the segment may be exposed to when the armature is dismantled. It is necessary, in fact, that the load-line should intersect with the demagnetisation curve at a point above the deflection in the latter; and this condition is just about satisfied for Magnadur 3 (improved version) at $\gamma \simeq 75°$. For these reasons it is always necessary to determine the working points, especially where the segment is flat and thin. The point of deflection is fairly high up on the demagnetisation curve of Magnadur 2 (improved version), and this means that there is no advantage in employing the material unless the magnetising operation is deferred until the armature is inserted. Nor must the armature be withdrawn from the motor afterwards.

Since these magnets have very high working points once the armature has been inserted, their thermal stability is also very good. Accordingly, there is no need to expect any decrease in the flux if the motor is subjected to low temperatures.

Flux Generated in the Motor under Load (Armature Reaction)

Armature reaction is the effect of the field created by the armature currents on the excited field, and the consequent changes in the magnitude and direction of the field in which the armature must operate. Saturation effects in those parts made of iron, such as in motors with electromagnetic field-excitation, are unlikely to become a problem in motors embodying permanent magnets, where flux densities are comparatively low and pole shoes are absent.

---

*These data relate to a graphical representation, in which the flux intensity (in gauss) is given on the same scale as the magnetic field (in oersted; 1 oersted representing 0·796A/cm).

Since the direction of the resulting field changes in accordance with the position of the brushes (which lie in the neutral zone when no current is flowing through the armature windings) the number of turns in the right position will also change cyclically. The effect is as if the neutral zone were being displaced by the armature field. The result is that the back e.m.f. appearing across the brushes is reduced, and it is not to any great extent affected by the fact that the excited field and the armature field together produce an increase in the maximum generated flux. The increase in flux values can be demonstrated experimentally.

No method has so far been found for directly measuring or calculating the flux actually passing through the windings under load. The true value can, however, be inferred by using the torque formula (Eq.(14)) in reverse, after measuring the actual torque delivered. Another indirect method is to determine the resistance R_t (see below), whereupon V_o can be evaluated from Eq.(12). The flux can then be calculated from Eq.(8). With the aid of these two methods it is possible to arrive at a reasonably reliable estimate of the flux actually effective in the motor.

We can take as an example a two-pole motor under load. It was found that at a speed of n = 1300 rev/min., at which speed the motor developed a torque of $M_n = 1940$ pcm, there was a roughly 10% fall-off in the flux relative to Φ_0. Under start-up conditions (with the armature blocked; the number of amp-turns was 1900) the apparent fall-off was as much as 17%. With a multi-pole motor there is less armature reaction per magnetic circuit, for the same total number of amp-turns, as is illustrated by the fact that there was found an approximately 3% fall-off in flux relative to Φ_0 in a motor built on the lines of Fig. 5n when it was run at a speed of n = 2000 rev/min.; and it developed a torque of $M_n = 34\,000$ pcm (number of amp-turns: 4630).

Determination of η_m

The coefficient of mechanical efficiency, $\eta_m = P_n/P_m$, is determined by iron losses and frictional losses, including windage loss. Frictional losses in the bearings and at the brushes are roughly proportional to speed so long as it remains fairly low; but windage losses are proportional, to a first approximation, to the square of the motor speed. Iron losses due to hysteresis and eddy currents occur in the armature core and iron frame. The hysteresis losses are proportional to the motor speed, the eddy current losses to the square thereof. In motors whose field excitation is provided by Magnadur magnets, no account need be taken of eddy current losses, because Magnadur has an extremely high electrical resistivity.

Thus the total frictional and iron losses, including windage loss, are covered by the expression:

$$P_v = P_{Friction} + P_{Iron} = C_1n + C_2n^2 + C_3n + C_4n^2 = \\ = C_5n + C_6n^2 \qquad \ldots(32)$$

where the C_v coefficients represent constants. The braking couple for which these losses are responsible is

$$M_v = \frac{P_v}{n} = C_5 + C_6n. \qquad \ldots(33)$$

On plotting this quantity as a function of motor speed, a straight line is obtained.

These losses can be more or less accurately estimated on the basis of empirical data, or on data given in handbooks, or both. Often, however, it is an easier matter to measure them on a test machine. This might take the form of a Magnadur-excited motor with spindle, commutator, and rotor dimensions of the same order as those in the motor to be designed. The braking couple $M_v = M_m - M_n$ is in fact quite easy to determine by letting the motor run unloaded (so that $M_n = 0$), for in these circumstances the whole of the delivered torque is needed to cover the losses in question. Eq.(3) implies that $\eta_m = 0$ in these circumstances, and it follows from Eq.(10) that

$$M_v = \frac{p}{a} z\Phi I_n . 1{\cdot}62.10^{-5}. \qquad \ldots(34)$$

where M_v is in pcm, Φ is in maxwell, I_n is in A.
The value of $pz\Phi/a$ can be easily found by measuring the voltage across the unloaded motor while it is being driven from an outside source; that is, while it is being operated as a dynamo. In these circumstances it can be inferred from Eq.(8) that:

$$\frac{p}{a} z\Phi = \frac{V_o.60.10^8}{n}. \qquad \ldots(35)$$

where Φ is in maxwell, V_o is in V, n is in rev/min.
The procedure is to measure the motor current and speed at different voltages. In this way it is possible to determine $I_n = f(n)$, and then to deduce $M_v = f(n)$ with the aid of Eq.(34). It is, of course, assumed here that the flux inside the unloaded machine operating as a dynamo is practically the same as that in the unloaded motor, the motor currents being kept very small.

Fig. 11 shows the results of I_n and M_v measurements done in this way. It will be noted that the plots obtained were in fact straight lines, as they are required to be by Eqs.(33) and (34).

Where the required useful torque M_n at a given speed n has been specified, M_m and η_m at that speed can be readily found:

$$\left.\begin{aligned} M_m &= M_n + M_v \\ \text{and} \quad \eta_m &= \frac{M_n}{M_n + M_v} \end{aligned}\right\} \qquad \ldots(36)$$

Any error in the determination of M_v will only partly affect the accuracy of η_m, in view of the fact that M_n is normally greater than M_v.

Determination of R_t

The total resistance R_t is made up of that of the armature windings R_a and that of the brushes R_b. The value of R_a can be found by measuring or calculating the resistance of the parallel current paths through the armature, but in so doing account must be taken not only of the type of winding employed, but also the width of the commutator bars and that of the brushes, as will now be explained.

If each brush is in contact with one commutator bar and one only, the overall armature resistance will have its maximum value. If, however, in certain positions of the commutator, two or more of the current paths through the armature are short-circuited, then in these positions the effect will be as if fewer windings are connected in series, and the armature resistance will be lower. In a case like this, one will have to determine what proportions of the total cycle are occupied by the two states, and work out a mean value accordingly. The difference between $R_{a\,max}$ and $R_{a\,min}$ can be quite appreciable, particularly for wave windings, or where the number of poles is fairly large, or where the commutator bars are few. A 30% difference between the two resistance values was found for a twelve-pole wave-wound motor with a rating of several hundred watts, and having a commutator made up of 37 bars.

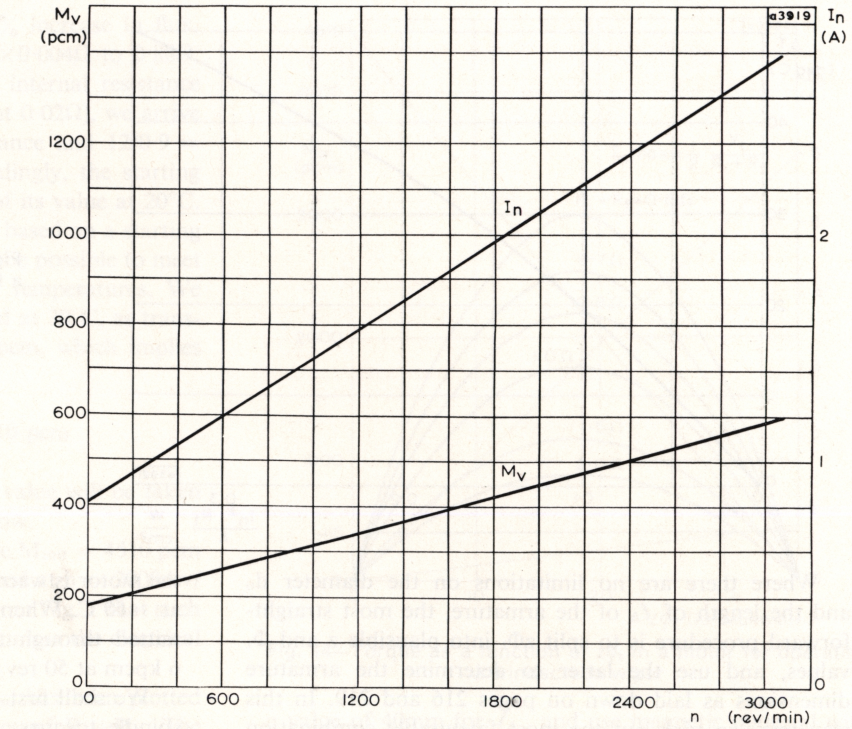

Fig. 11—Measured current (I_n) through unloaded motor, and torque developed (M_v), as functions of motor speed

Spindle diameter	9·5mm
Commutator diameter	19 mm
Armature length	25 mm
Armature diameter	56·1mm

It should be added that the resistance value thus found must be adjusted to the armature operating temperature.

The total brush resistance R_b is made up of that of the brushes themselves and that of the contact between brush and commutator. Metal-carbon brushes are widely used, and their resistivity is of the order of $10^{-5}\Omega$cm. In most cases, then, the resistance of the brushes can be neglected.

Manufacturers usually specify the voltage drop occasioned by the contact between brush and commutator, instead of the resistance of the contact. For metal-carbon brushes, the brush drop is of the order of 0·2V to 0·6V. This yields the following value for the contact resistance:

$$R_b = \frac{2V_b}{I_n} = \frac{2.0{\cdot}4}{I_n}.$$

This voltage drop is independent of current or, more accurately, independent of current density, over a wide range; that is to say, R_bI_n is constant. It is, however, affected by the motor speed and brush pressure, though no exact information is available on this. The higher the pressure, the smaller is the influence that the motor speed has on the contact resistance. For this reason it is wise to measure the total motor resistance both as a function of motor current and as a function of motor speed. The results of such measurements are shown in Fig. 12.

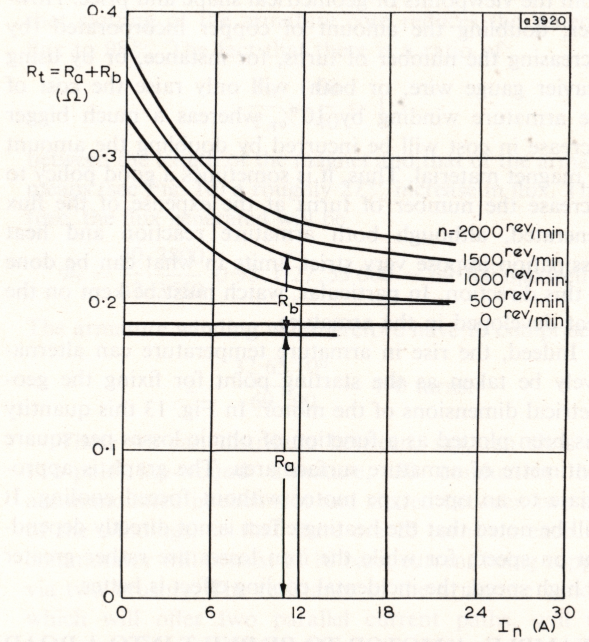

Fig. 12—Total motor resistance versus current, at various speeds. Brush cross-section 6·3×6·3mm, brush pressure 150p/cm², spindle diameter 9·5mm, commutator diameter 19mm

Dimensioning the Armature: diameter and length

The calculations carried out earlier result in a value $z\Phi_t$ which the designer has to obtain from his motor, given a certain value of R_t. Together, R_t and z determine the amount of copper that will have to be used, and Φ_t fixes the amount of magnetic material needed.

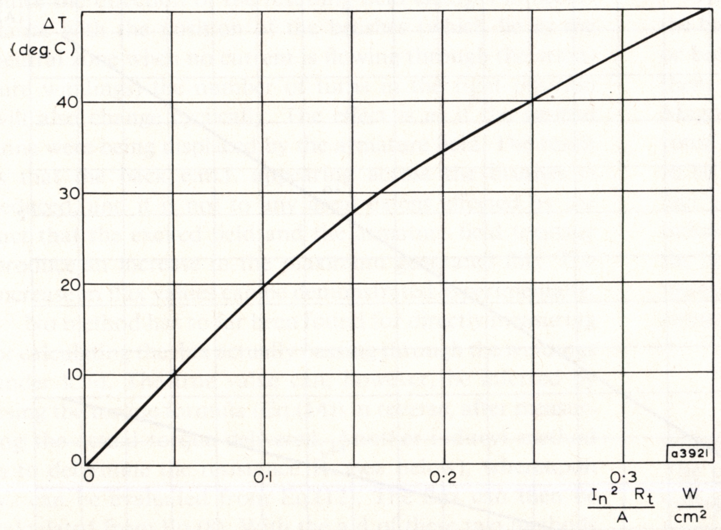

Fig. 13—Armature temperature rise as a function of ohmic losses per cm² of armature surface area A

Where there are no limitations on the diameter d_o and the length of ℓ_A of the armature, the most straightforward procedure is to split $z\Phi_t$ into plausible z and Φ_t values, and use the latter to determine the armature dimensions as laid down on pages 216 and 219. In this way one can pick out the most favourable combination from the viewpoints of geometrical shape and price. However, doubling the amount of copper incorporated (by increasing the number of turns, for instance, or by using heavier gauge wire, or both) will only raise the cost of the armature winding by 10%, whereas a much bigger increase in cost will be incurred by doubling the amount of magnet material. Thus, it is sometimes a good policy to increase the number of turns at the expense of the flux generated, although both armature reaction and heat dissipation impose very strict limits in what can be done in this direction. In particular, watch must be kept on the heat developed in the armature.

Indeed, the rise in armature temperature can alternatively be taken as the starting point for fixing the geometrical dimensions of the motor. In Fig. 13 this quantity has been plotted as a function of ohmic losses per square centimetre of armature surface area. The graph is appropriate to an open type motor without forced cooling. It will be noted that the heating effect is not directly dependent on speed, for while the iron losses are rather greater at high speed, the incidental cooling effect is better.

EXAMPLE: A MOTOR TO BE BUILT INTO A ROAD VEHICLE

The method described will be illustrated by dimensioning a motor for use in road vehicles, on the basis of a few specifications relating to torque developed at various temperatures and the geometrical dimensions that the motor must have. A further requirement is that it shall run on a 12V supply.

At room temperature (20°C) the starting torque transmitted by reduction gearing with a ratio of 1:40 has to be at least $M_o' = 100$kpcm. The efficiency of the gearing can be taken to be about $\eta_{gear} = 0{\cdot}6$. In an actual case, the efficiency of the mechanical transmission was found to be 65%. The starting torque must be at least 80kpcm when the motor is warm (at about 70°C), and at least 120 kpcm at −10°C. When the motor is running, the torque transmitted through the reduction gearing must be at least 6 kpcm at 50 rev/min. and 20°C.

We shall first convert the above values into the actual spindle torques, assuming that the mechanical efficiency η_m is close to unity during start-up and falls off to 0·6 when the motor is running steadily. This assumption is justified by measurements on other motors. Taking a value of 0·97 for η_m during start-up, we find that the starting torque will be

$$M_{m0} = \frac{10^5}{0{\cdot}6\,.\,40\,.\,0{\cdot}97} = 4300\text{pcm at } 20°\text{C}$$

$$M_{m0} = \frac{0{\cdot}8\,.\,10^5}{0{\cdot}6\,.\,40\,.\,0{\cdot}97} = 3440\text{pcm at } 70°\text{C}$$

$$M_{m0} = \frac{1{\cdot}2\,.\,10^5}{0{\cdot}6\,.\,40\,.\,0{\cdot}97} = 5150\text{pcm at } -10°\text{C}.$$

During steady running at a speed of n = 2000 rev/min. the torque will be

$$M_m = \frac{6000}{0{\cdot}6\,.\,40\,.\,0{\cdot}6} = 416\text{pcm}.$$

The next step is to ascertain whether the demands relating to percentage increases and decreases in torque at different temperatures can be met. The starting torque is proportional to Φ and I_o(Eq.(10)), which are temperature-dependent. We shall have to determine these temperature functions, starting from the torque required at 20°C. The total resistance R_t presented by the motor will be provisionally put at 1Ω. The internal resistance of the accumulator, being $R_i \simeq 0{\cdot}01\Omega$ and therefore small compared with R_t, can safely be neglected. This being so, the starting current I_o will be 12A (at 20°C; $V_L = 12$V).

The flux generated at 70°C is $50 \times 0{\cdot}2 = 10\%$ less than that at 20°C, for the temperature coefficient of magnetic induction is $0{\cdot}2 \times 10^{-2}$ per degC. At the same time R_t increases by $50 \times 0{\cdot}004\Omega$ to $1{\cdot}2\Omega$, the temperature coefficient of the resistivity of copper being 0·004Ω/degC. At 70°C, then, I_o is only 10A, and this reduces the starting torque to 0·9(10/12) = 75% of its value at 20°C.

At −10°C there is a $30 \times 0{\cdot}2 = 6\%$ increase in flux, but the resistance R_t decreases by $30 \times 0{\cdot}004\Omega$ to 0·88Ω. Allowing for a slight increase in the internal resistance of the accumulator (to a value of about 0·02Ω), we arrive at values of 0·9Ω for the total resistance and 12/0·9 = 13·4A for the starting current. Accordingly, the starting torque will be 1·06(13·4/12) = 118% of its value at 20°C.

It is clear, then, that if the design is based on a starting torque of 4300 pcm at 20°C, it will not be possible to meet the demands for the torque at other temperatures. We shall therefore raise the torque required at 20°C, as transmitted through the gearing, to 105 kpcm, which implies a torque of

$$M_{m0} = \frac{1{\cdot}05\,.\,10^5}{0{\cdot}6\,.\,40\,.\,0{\cdot}97} = 4510 \text{ pcm}$$

acting on the spindle at start-up. This value will be taken as a basis for the calculations that follow.

The ratio between the starting torque $M_{m0} = 4510$ pcm and the torque $M_m = 416$ pcm developed at n = 2000rev/min. is very high; and it will be clear from Fig. 1 that such a ratio will not be feasible in practice unless the electrical efficiency is very high.

In Fig. 14, as in Fig. 1, torque M_m has been plotted as a function of $z\Phi_t$ for various values of R_i+R_t. The curves are based on Eq.(14) ($V_L = 12$V, n = 2000 rev/min.). From Eq.(15) we can infer that the maximum torque is obtained with,

$$z\Phi_t = \frac{12}{2000}\cdot 3\,.\,10^9 = 18\,.\,10^6 \text{ maxwell}.$$

The straight line corresponding to $M_m = 416$ pcm has been drawn in Fig. 14, as also has that corresponding to the starting torque $M_{m0} = 4510$ pcm (see page 214). The point at which these lines intersect would lie on a curve relating to an R_i+R_t value of about 1·44Ω, the corresponding $z\Phi_t$ value being $32{\cdot}65 \times 10^6$ maxwell. This in its turn corresponds to an electrical efficiency of η_e = 32·65/36 = 90·6%. This produces an I_n value of 0·786A.

We shall now have to find out whether this very high $z\Phi_t$ value can be obtained from a motor of conventional design. Of course, in these circumstances a very high Φ_t is desired, and one way of getting it would be to choose a four-pole design. However, for the time being we shall try to suit the requirements with a two-pole motor.

Let us now write down one or two plausible geometrical dimensions for the magnetic circuit and see whether they allow the desired $z\Phi_t$ to be obtained (see also Fig. 6).

d_i = 44mm (inside diameter of the magnetic segments)
ℓ_M = 60mm (length of the segments)
h = $(d_a - d_i)/2$ = 8mm (wall thickness of the segments)
h_{Fe} = 5mm (wall thickness of iron frame)
β = 120° (angle subtended by one segment).

The values chosen above fix the overall diameter of the motor and the width of the air gap:

D = 70mm s = 0·3mm

We see from Fig. 9 that a pair of transversely magnetised segments will generate a $z\Phi_t$ of 55 000 maxwell for an unslotted armature having a length of 42mm. Let us adopt a value of 40mm for ℓ_A, and use magnetic material with a remanence of 3800×10^{-8} Vs/cm². We shall assume that slotting of the armature core reduces the generated flux to 98%. The fact that there is a ratio of:

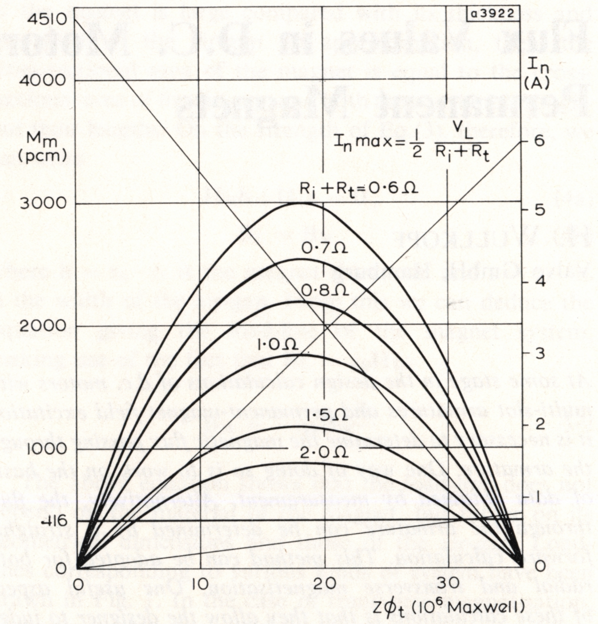

Fig. 14—Torque as a function of $z\phi_t$ in a motor for operating a windscreen wiper

$$\frac{\ell_M}{\ell_A} = \frac{60}{40} = 1{\cdot}5$$

between the length of the magnet and that of the armature means (see Fig. 10) a roughly 27% increase in flux. Therefore, the flux generated will be

$$\Phi_t = \frac{40}{42}\cdot\frac{3800}{3550}\cdot 0{\cdot}98\,.\,1{\cdot}27\,.\,55\,000 = 69\,700 \text{ maxwell}.$$

The armature winding will therefore have to comprise

$$z = \frac{32{\cdot}65\,.\,10^6}{69\,700} = 470 \text{ turns}.$$

These we can distribute between, say, ten slots in a two-pole lap-wound armature, 50 conductors being accommodated in each slot and shared between two sides of the windings, so that there are 25 turns on each. The commutator will consist of 10 bars, current being supplied via two brushes. The resistance of the armature winding, which will offer two parallel current paths, will then amount to about 0·75Ω. If we use 0·5mm gauge wire, the aggregate cross-sectional area of the copper in one slot will be $50\ (\pi/4) \times 0{\cdot}5^2 \simeq 10\text{mm}^2$. Estimating the filling factor at 0·3, we can say that the slots will have to have a cross-sectional area of about 35mm². Ten slots measuring 5mm × 7mm (say) can easily be cut in an armature core whose diameter is 40mm, and it might be worthwhile considering whether the geometrical dimensions of the motor can be further reduced. It would, in fact, be quite feasible to reduce the motor diameter from 70mm to 63mm, and the armature diameter from 43·4mm to about 40mm. The amount of heat dissipated in the armature is so small in the present case that it need not be taken into account.

Flux Values in D.C. Motors embodying Magnadur Permanent Magnets

H. WULLKOPF
Valvo GmbH, Hamburg

At some stage in the design calculations of d.c. motors with multi-slot armatures and permanent-magnet field excitation it is necessary to determine the magnetic flux passing through the armature. One way of doing so is to work on the basis of data obtained by measurement. Alternatively, the flux through the armature can be determined by a straight-forward calculation. This method can be adopted for both radial and transverse magnetisation. One useful aspect of these calculations is that they allow the designer to judge the suitability, in a given motor, of the various types of Magnadur and the various kinds of magnetisation.

INTRODUCTION

The object of this article is to determine the flux passing through the unslotted iron armature in a system embodying ring field-magnets or segments made of Magnadur, from given data comprising the magnetic characteristics and geometrical dimensions of the system. This purely mathematical method of flux determination can be employed alongside the graphical procedure described by Reynst (Ref. 16), which is based on measurement. As will be shown, the two methods yield practically the same result. The procedure described by Reynst can in any case be employed for working out other motor characteristics.

MAGNETISATION PATTERNS

Ring magnets or segments to be embodied in d.c. motors are magnetised either radially or transversely. Radial magnetisation with a square-wave will result in a motor with a high torque, and there is also much to be said for radial magnetisation with a sinusoidal fundamental plus 3rd harmonic (Ref. 15), but only where the motor is small and is equipped with a three-pole armature. The latter case will not be further considered in the present article.

Generally speaking, it is with square-wave radial magnetisation that the highest possible magnetic flux is obtained, and this therefore is the method chosen. However, materials are available which can be so treated that they acquire a bias toward magnetisation in a certain direction. These cannot be oriented in a radial pattern except with difficulty, so transverse magnetisation is usually chosen because it simplifies production. Moreover, it may be necessary, for constructional reasons, to defer magnetisation until after the motor is assembled; at present the transverse method is the only form of magnetisation feasible.

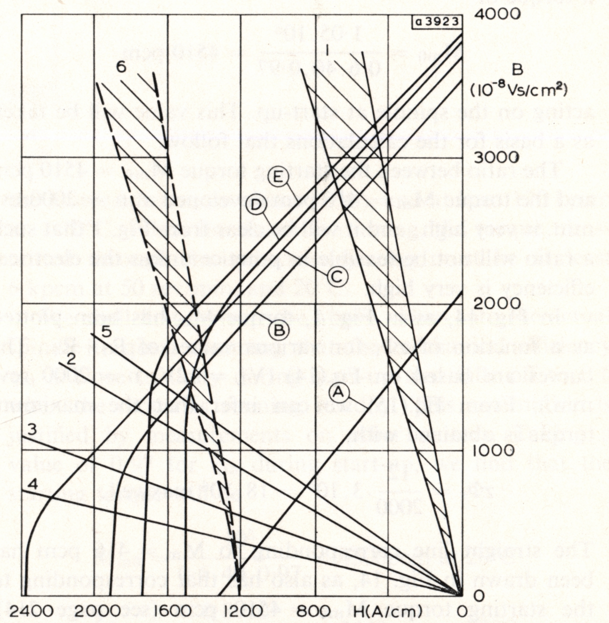

Fig. 1—Demagnetisation curves of different Magnadur grades (indicated by A, B, C, D, E), with loadlines of magnet systems in assembled and dismantled states (1, 2, 3, 4, 5, 6). The loadlines relate to a motor with an armature of diameter $d_0 = 52{\cdot}5$mm

Magnadur grades
A: Magnadur 1
B: Magnadur 3
C: Magnadur 3 (improved version)
D: Magnadur 2
E: Magnadur 2 (improved version)

1. Working zone of the assembled system
2. Radially magnetised ring magnet with surround ring but no armature
3. Radially magnetised ring magnet with neither surround ring nor armature
4. Transversely magnetised 120° segment without armature or backing
5. Transversely magnetised segment twice the thickness of that in (4), without armature or surround ring
6. Working zone of assembled system when placed in reverse field of 1200A/cm created by the short-circuit current through the armature

Fig. 1 displays the demagnetisation curves of a number of Magnadur materials. That of Magnadur 1, as also those of the preferentially-oriented materials, insofar as the sections above the points of deflection are considered, approximate very closely to straight lines. These curves or sections of curves can accordingly be represented (Koch and Wullkopf, Ref. 15) by the equation

$$B_M = \mu_0\mu_{rev}H_M + B_r\,, \qquad \ldots(1)$$

where μ_{rev} is the reverse permeability, B_r the remanence, and B_M and H_M are the flux density and field strength in the magnet.

The total flux can be arrived at by integrating the magnetic induction over one entire pole-face. In so doing we shall assume that the lines of magnetic induction distributed unevenly around the circular system all lie in radial directions. We assume, in fact, that the amount of flux passing through the armature is the same as that issuing from one pole face. Let the pole face extend over an angle β (say from β_1 to β_2), and let the armature and the magnet have the same length ℓ, the inside radius of the magnet being r_i. We then have:

$$\Phi = r_i\ell\int_{\beta_1}^{\beta_2} B_L(\phi)d\phi\,. \qquad \ldots(2)$$

Obviously, it does not matter here whether the field magnet is a complete ring (so that $\beta_1 = 0$, $\beta_2 = \pi$) or consists instead of two separate segments each subtending an angle $\leqslant \pi$.

We shall further have need of two fundamental laws for calculating flux, irrespective of whether the system is radially or transversely magnetised. These are

$$\oint H ds = 0 \qquad \ldots(3a)$$

and

$$\operatorname{div} B = 0. \qquad \ldots(3b)$$

Radial Magnetisation

Fig. 2 represents a cross-section through an experimental arrangement embodying an unslotted armature; the lines of induction are also shown. In general, the radius of the magnet is large compared with its thickness and the width of the air-gap. In approximation, then, the cross-sectional area of the magnet is equal to the cross-sectional area of the air-gap, and both are constant throughout their lengths. On the strength of Eq.(3), therefore, we can write

$$H_M h + H_L s = 0\,, \qquad \ldots(4a)$$

$$B_L = B_M\,. \qquad \ldots(4b)$$

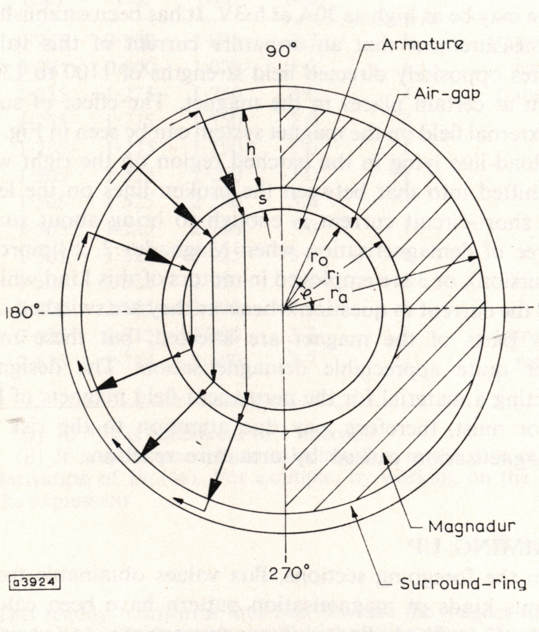

Fig. 2—Lines of induction in a radially magnetised experimental arrangement with an unslotted armature

where $h = r_a - r_i$ is the magnet thickness, and $s = r_i - r_o$ is the width of the air-gap. From this we can deduce the equation giving the load-line of the magnet system, making use of the fact that $B_L = \mu_0 H_L$:

$$B_M = -\mu_0 H_M \frac{h}{s}\cdot \qquad \ldots(5)$$

The above equation shows that the load-line does not depend on the material of the magnet, but rather on its geometrical dimensions and those of the air-gap. Load-lines corresponding to various kinds of system have been drawn in Fig. 1. In the case of transverse magnetisation, of course, each particle of the magnet has its own load-line. The working point of a given particle in the magnet is given by the intersection of the load-line for that particular particle (Eq.(5)) with the demagnetisation curve (Eq.(1)). It follows from Eqs.(1), (4) and (5), that,

$$B_L = B_M = \frac{B_r}{1+\mu_{rev}\frac{s}{h}}\cdot \qquad \ldots(6)$$

We can now determine the flux value by simply inserting the above expression in Eq.(2). If β is the angle subtended by a segment to the centre of the system (for a ring magnet, $\beta = \pi$) then *

$$\Phi = \frac{B_r r_i \ell\beta}{1+\mu_{rev}\frac{s}{h}}\cdot \qquad \ldots(7)$$

Transverse Magnetisation

A cross-section through an experimental set-up comprising a transversely magnetised unslotted iron armature together with the appropriate lines of induction, appears in Koch and Wullkopf (Ref. 15) as Fig. 12. It will be seen from this diagram that, provided the air-gap is narrow, the induction and field-of-force lines therein have a virtually radial orientation, allowing us to establish the following relationship between flux densities in the air-gap and the magnet material:

$$B_L = B_M \sin\phi. \qquad \ldots(8)$$

It will also be seen that the magnetic path length is dependent on the angle ϕ. However, in calculating the flux created by thin ring magnets ($h \ll r_i$) this fact can be ignored, seeing that the dependence of path length on ϕ only becomes really marked in the regions around $\phi = 0$ and $\phi = \pi$, and very little flux issues from these particular regions of a transversely magnetised ring. Taking Eq.(4a), from the calculations relating to a radially magnetised system, and Eqs.(1) and (8), we get:

---

*See footnote under Table 2 (page 227).

$$B_L = \frac{B_r \sin\phi}{1+\mu_{rev}\frac{s}{h}\sin\phi}\,. \qquad \ldots(9)$$

To simplify matters when integrating, let us take the factor $\sin\phi$ in the numerator to be unity; the adjustment is only of very minor importance in the expression as a whole because, in most practical cases, s/h is much less than unity, and the smallest deviations again occur in the regions around $\phi = 0$ and $\phi = \pi/2$. As already stated, practically no flux issues from these regions. When this is done, Eq.(9) becomes identical with Eq.(93) in Koch and Wullkopf (Ref. 15), provided that we put $\psi_{0v} = 0$ in the latter equation (in the absence of an energising current through the armature). It should also be noted that the derivation of Eq.(9) has been based on the same assumption as that of Eq.(93) in Ref. 15.

The total flux generated can now be evaluated by inserting Eq.(9) in Eq.(2). Regarding the segments as symmetrically arrayed about $\phi = \pi/2$ and $\phi = 3\pi/2$, and integrating over the angle β subtended by a segment, we obtain

$$\Phi = \frac{2B_r r_i \ell \sin\frac{\beta}{2}}{1+\mu_{rev}\frac{s}{h}}\,. \qquad \ldots(10)$$

DEMAGNETISATION EFFECTS

In the course of the above calculations it has been assumed that the magnetisation was stable; that is to say, it could not change irreversibly in consequence of dismantling, armature reaction, or other influences. The assumption is quite justified where the magnets are made of materials like Magnadur 1 or 3 (improved version); but difficulties may arise from the use of certain preferentially-oriented materials, as will now be explained.

When a ring magnet has been magnetised before the insertion of the armature (which is normal practice for radially-magnetised systems), the magnet is loaded with the reluctance of the entire air-space it encloses. It is additionally loaded with that of the surrounding air if the iron ring that completes the outside circuit has not yet been fitted. The same situation arises when the armature is subsequently withdrawn from a motor that has undergone transverse magnetisation. In these circumstances the load-line is flatter than with the complete assembly, with the result that the ring magnet has a working point on the lower part of its demagnetisation curve. When the system is subsequently assembled the desired working point will not be attained unless the portion of the demagnetisation characteristics being studied is linear. If there is a knee in this part of the curve, the flux density will be lower. The following example shows how far one can safely go in dismantling motors embodying various kinds of ring magnet or segments without incurring an irreversible loss of field strength.

Fig. 1 shows the demagnetisation curves of the ceramic materials Magnadur 1, 2, 2 (improved version), 3, and 3 (improved version). Since the load-line of a system is dependent only on its geometrical dimensions (Eq.(5)), it does not matter which material is embodied in the system whose load-line is to be determined. The load-line thus found will be valid for that particular system irrespective of the type of magnet material employed, provided that the magnet dimensions are the same as, or proportional to, those of the magnet being studied. The hatched region on the right of Fig. 1 is the working zone of a ring magnet in the complete motor assembly; it relates to an armature diameter of 52·5mm and a ring magnet with an outside diameter of 70mm and inside diameter of between 53·3 and 54·7mm. Also shown in Fig. 1 are measured load-lines for the ring magnet with its armature, but without its iron surround-ring (the motor housing), and for the magnet minus both armature and surround-ring.

In addition, a measured load-line for a single 120° segment without surround-ring has been shown. The segment was cut from a ring with dimensions as stated above; two such segments are usually incorporated in the motor. Finally, Fig. 1 shows the load-line of a segment twice as thick as the other magnets (h ≃ 15·5mm), intended to be paired with an iron segment which is mounted on the other side of the armature.

It will be clear from Fig. 1 that any material with a linear demagnetisation characteristic, such as Magnadur 1, can be magnetised before assembly, whereas caution must be exercised in dealing with preferentially-oriented materials. Magnadur 2 has so low a coercivity that it must be magnetised when inside the finished assembly. Partial dismantling is permissible in certain circumstances for motors with field magnets made of Magnadur 3; but the surround ring must never be removed.

As well as the danger of irreversible demagnetisation caused by dismantling, there is that of an irreversible weakening of the magnet by the oppositely directed field produced by the short-circuit current through the stalled armature. For example, in a windscreen-wiper motor that is widely available commercially, this short-circuit current value may be as high as 30A at 6·3V. It has been established by measurement that an armature current of this value creates oppositely directed field strengths of 1100 to 1300 A/cm at certain places in the magnet. The effect of such an external field on the magnet system can be seen in Fig. 1: the load-line lying in the hatched region on the right will be shifted into that between the broken lines on the left. The short-circuit current is enough to bring about some degree of demagnetisation when Magnadur 2, 2 (improved version), or 3 are employed in motors of this kind, which pass the current in question whenever they are switched on. Only parts of the magnet are affected, but these may suffer quite appreciable demagnetisation. The designer selecting a material for the permanent-field magnets of his motor must, therefore, pay due attention to the risk of demagnetisation caused by armature reaction.

SUMMING UP

In the foregoing sections, flux values obtainable from various kinds of magnetisation pattern have been calculated. Calculated flux values appropriate to various materials and magnetisation patterns have been collected

TABLE 1

Flux values obtainable from systems made of different Magnadur materials that have undergone various kinds of magnetisation. The values listed are relative to the flux obtained, after assembly in a motor, from a Magnadur 1 ring magnet that has undergone radial-magnetisation over two diametrically-opposed 120° arcs. All values are appropriate to a motor with an unslotted armature of diameter d_0 = 52·5mm and an air-gap of s = 0·5mm.

Magnadur	Form (Shape)	$B_r(10^{-8}$Vs/cm$^2)$	Magnetisation	Relative Flux value
1	Ring	2000	radial	1
1	Segment, β = 120°	2000	,,	0·68
X	Ring	3700	transverse	1·20(i)
X	Ring	3700	radial	1·85(i)
X	Segment, β = 120°	3700	,,	1·26(i)
X	Segment, β = 140°	3700	,,	1·47(i)
	Segment, β = 140°	2650	,,	1·06(ii)
	Segment, β = 140°	3300	,,	1·31(ii)
3	Ring	3550	,,	1·78(i)
3	Segment, β = 120°	3550	,,	1·22(i)
3	Segment, β = 140°	3550	,,	1·43(i)
2	Ring	3850	transverse	1·26(iii)
2	Segment, β = 120°	3850	,,	1·08(iii)

(i) Difficulty of manufacture places limitations on the size of these magnets.

(ii) Materials having some degree of preferential orientation.

(iii) Magnadur 2 has too low a BH_c value for use as field-magnet material in motors.

TABLE 2

Calculated, compared with measured, flux values for systems with different geometrical dimensions, embodying magnets of various materials that have undergone different kinds of magnetisation.

r_o (cm)	r_i (cm)	r_a (cm)	ℓ (cm)	Magnadur	Magnetisation	$\frac{B_r}{1+\mu_{rev}\frac{s}{h}}$ $(10^{-8}$Vs/cm$^2)$	Φ calculated for β = 175° $(10^{-8}$Vs)(i)(ii)	Φ measured $(10^{-8}$Vs)(i)	$\frac{\Delta\Phi}{\Phi \text{ calculated}}$ (%)
0·765	0·800	1·075	1·2	1	transverse	1740	3340	3100	−7
0·765	0·800	1·075	1·2	1	radial	1740	5100	5200	+2
1·255	1·275	1·750	3·0	3	transverse	3390	25900	24000	−8
1·255	1·275	1·750	2·0	3	,,	3390	17300	15900	−8
1·255	1·275	1·750	3·0	1	,,	1900	14600	12700	−13
1·505	1·525	2·250	3·0	1	,,	1940	17700	17000	−4
1·505	1·525	2·250	3.0	3	,,	3440	31500	28000	−11
1·505	1·525	2·750	3·0	1	,,	1960	18000	16000	−11
1·505	1·525	1·925	3·0	1	,,	1890	17300	15800	−9
1·505	1·525	2·250	3·0	1	radial	1940	27100	26000	−4
2·500	2·585	3·500	2·5	1	,,	1800	35600	38000	+7
2·625	2·715	3·500	3·3	1	transverse	1765	31600	28900	−9
2·625	2·715	3·500	3·3	1	radial	1765	48300	46900	−3

(i) 10^{-8}Vs is equivalent to 1 maxwell.

(ii) It is quite possible to calculate flux in the case of radial magnetisation without making the assumption underlying the derivation of Eq.(4a). For example, by working on the basis of Eq.(20) in the article by Koch and Wullkopf one arrives at the expression

$$\Phi = \frac{B_r h \ell \beta}{\ln\frac{r_a}{r_i} + \mu_{rev}\ln\frac{r_i}{r_o}}\,.$$

This readily transforms into Eq.(7) where the magnet thickness and gap-width are small. The above expression, as it stands, generally yields flux values still higher than those obtained from Eq.(4a), although the difference is small. The fact that the measured flux is always lower than the calculated value can be explained by assuming that there are slight deviations from the ideal pattern on which the calculations are based. The calculated values are to be considered rather as theoretical maxima.

together in Table 1 to allow convenient comparison. The calculations were based on the remanence values of the materials in question, as specified in column 2 of the table. The flux values shown are relative to that obtained from a radially-magnetised Magnadur ring magnet, this being allotted a value of unity.

The table makes it clear that square-wave radial magnetisation is superior to any other kind in regard to the flux obtainable from the resulting system. It should, however, be pointed out that an exactly radial magnetisation pattern is impossible to achieve in practice, although deviations from the strict pattern are confined to a narrow segment of the circular system (covering about 10°). The deviations are less marked where the system is not unduly small.

The production of Magnadur rings with preferential orientation in a radial pattern is a very difficult matter, since the material undergoes much greater contraction in the preferential direction than in the direction perpendicular thereto, with the result that extremely severe stresses may be set up in the rings. Moreover, the possibility of irreversible demagnetisation later on (Fig. 1) has always to be borne in mind.

In order to check the calculations carried out in respect of the various kinds of magnetisation, a series of ring magnets was investigated and the measured values compared with the calculated ones. These values appear side by side in Table 2. The measurements confirmed that the calculations have a degree of accuracy quite adequate for permanent magnets, for both radial and transverse magnetisation. It will be further noted that, as a rule, values calculated for systems embodying unslotted armatures, and using iron of infinitely high permeability, are somewhat in excess of true values. The designer should therefore subtract about 7% from the calculated flux to allow for leakage and the losses brought about by the slotting of the armature.

The magnetic-induction formulas worked out in the preceding section in respect of the two magnetisation patterns and flux formulas that they lead to, are subject to the proviso that both the gap width and the thickness of the magnet must be small compared with the magnet's radius. Now, this is always so in motors of normal design. If there is any definite departure from conventional design, so that the air-gaps become abnormally wide or the walls of the ring magnets abnormally thick, then Eqs.(7) and (10) cannot be used, because the approximations underlying them are not then justified. Moreover, much more importance must be attached, in these circumstances, to deviations from the ideal magnetisation pattern and to leakage flux from the end-faces of the magnets. These factors have not been considered in this article.